Summertime changes in climate extremes over the peripheral Arctic regions after a sudden sea ice retreat

Steve Delhaye [1], Thierry Fichefet [1], François Massonnet [1], David Docquier [2], Rym Msadek [3], Svenya Chripko [3], Christopher Roberts [4], Sarah Keeley [4], and Retish Senan [4]

[1]Georges Lemaître Centre for Earth and Climate Research, Earth and Life Institute, Université catholique de Louvain, Louvain-la-Neuve, Belgium
[2]Royal Meteorological Institute of Belgium, Brussels, Belgium
[3]CECI, Université de Toulouse, CNRS, CERFACS, Toulouse, France
[4]European Centre for Medium-Range Weather Forecasts, Shinfield Park, Reading, RG2 9AX, UK

Correspondence: Steve Delhaye (steve.delhaye@uclouvain.be)

Abstract. The retreat of Arctic sea ice is frequently considered as a possible driver of changes in climate extremes in the Arctic and possibly down to mid-latitudes. Despite the existence of many studies, it is still unclear how the atmosphere will respond to a near-total retreat of summer Arctic sea ice, a reality that might occur in the foreseeable future. This study explores this question by conducting sensitivity experiments with two global coupled climate models run at two different horizontal resolutions to investigate the change in temperature and precipitation extremes during summer over peripheral Arctic regions following a sudden reduction in summer Arctic sea ice cover. An increase in frequency and persistence of maximum surface air temperature is found in all peripheral Arctic regions during the summer when sea ice loss occurs. For each million km^2 of Arctic sea ice extent reduction, the absolute frequency of days exceeding the surface air temperature of the climatological 90th percentile increases by $\sim$4% over the Svalbard area, and the duration of warm spells increases by $\sim$1 day per month over the same region. Furthermore, we find that the 10th percentile of surface daily air temperature increases more than the 90th percentile, leading to a weakened diurnal cycle of surface air temperature. Finally, an increase in extreme precipitation, which is less robust than the increase in extreme temperatures, is found in all regions in summer. These findings suggest that a sudden retreat of summer Arctic sea ice clearly impacts the extremes in maximum surface air temperature and precipitation over the peripheral Arctic regions with the largest influence over inhabited islands such as Svalbard or Northern Canada. Nonetheless, even with a large sea ice reduction in regions close to the North Pole, the local precipitation response is relatively small compared to internal climate variability.

1 Introduction

Arctic sea ice extent has been decreasing since the beginning of satellite observations in 1979. This decrease has occurred in all seasons but is more pronounced in late summer. In particular, September sea ice extent has shrunk by about 50% since the beginning of the satellite era (Onarheim et al., 2018). The loss of sea ice, which is largely attributed to the accumulation of greenhouse gases in the atmosphere following anthropogenic emissions (Notz and Stroeve, 2016; Screen et al., 2018) but also

to internal climate variability (Ding et al., 2017), has been proposed as a key driver of the "Arctic Amplification" (AA) through changes in albedo (Manabe and Stouffer, 1994; Screen and Simmonds, 2010) and other temperature-related feedbacks (Pithan and Mauritsen, 2014).

To investigate the role of the sea ice retreat on climate, observations are not sufficient (Smith et al., 2019). Indeed, sea ice and atmospheric circulation might be related to each other in the observational record, but this relationship could have occurred by chance. The relationship could also be non-causal, especially if both sea ice and the atmospheric circulation are driven by a common factor (Blackport et al., 2019). To overcome these problems, the use of numerical model experiments, in which a retreat of summer Arctic sea ice can be imposed, is an attractive approach to determine the influence of sea ice anomalies on the climate system. However, even with exactly the same experimental setup, significant differences in the mid-latitude responses are found within the same model, suggesting that internal climate variability to Arctic sea ice loss can play a large role (Peings et al., 2021).

The winter climate response to a summer Arctic sea ice loss and/or the AA have garnered a lot of attention (e.g. Francis and Vavrus, 2012; Cohen et al., 2014; Barnes and Screen, 2015; Cohen et al., 2020). So far, these responses have essentially been studied for mid-latitude regions (Ogawa et al., 2018). A debate also exists on the responses in summer at mid-latitudes, when the role of the stratosphere is almost non-existing (Kidston et al., 2015), due to a large uncertainty on dynamical aspects (Coumou et al., 2018). However, the climate response near the regions of Arctic sea ice loss depends primarly on the surface heat flux changes (e.g. Deser et al., 2010) and is therefore less dependent on the internal climate variability than at mid-latitudes. Thereby, the signal (response of the atmosphere to sea ice loss) to noise (internally generated variability) ratio over the peripheral Arctic regions is larger and less ensemble members are needed to get a significant response compared to mid-latitude regions (Screen et al., 2014). However, studies about the summer response fo the atmosphere to sea ice reductions and/or AA have been restricted to mid-latitude regions (Horton et al., 2016; Coumou et al., 2018).

In summer, the dynamical and thermodynamical aspects could move in the same direction leading to more extreme weather events such as hot extremes (Horton et al., 2016). An increase of climate extremes (frequency, intensity or persistence) can have greater impacts on human activities and on the natural environment than an increase in the climatic mean (Kunkel et al., 1999). Over the last decades, extreme heat events have increased in the Arctic regions mainly over the Arctic North America and Greenland (Matthes et al., 2015; Dobricic et al., 2020) and Arctic aridity has decreased (Meredith et al., 2019). These changes are already impacting the Arctic regions with a change in fish stocks (Hollowed et al., 2013; Haug et al., 2017) and in agriculture (Stevenson et al., 2014), and posing risks to local communities (Ford et al., 2008). Moreover, a "new Arctic" climate could even emerge during this century (Landrum and Holland, 2020). Indeed, a larger decrease of magnitude in cold extremes compared to the increase in warm extremes and an increase in precipitation extremes are expected over high latitudes (Kharin et al., 2013; Sillmann et al., 2013b). The projected Arctic sea ice loss could be responsible for this decrease in temperature variance (Blackport et al., 2021) and in the increase in precipitation extremes, but with a significant difference between regions

(Screen et al., 2015).

Even if the rate of summer Arctic sea ice decline is not uniform and might be slowed down for a few years depending on the effect of internal climate variability (Swart et al., 2015), sudden reductions in Arctic sea ice extent are likely to be more frequent in the future with sea ice retreating 4 times faster than the long-term trend (Holland et al., 2006). Moreover, many state-of-the-art climate models project a summer ice-free Arctic conditions before 2050 (SIMIP, 2020). The peripheral Arctic regions will be the first regions to be affected by a sudden sea ice retreat.

In this study, we investigate how the maximum surface air temperature and precipitation extremes over the Arctic regions in summer respond to a large sudden Arctic sea ice loss. To answer this question, outputs from two coupled general circulation models (GCMs) that participated in the High Resolution Model Intercomparison Project (HighResMIP; Haarsma et al. (2016)), at two different horizontal resolutions, and contributing to the EU Horizon 2020 PRIMAVERA project (PRocess-based climate sIMulation : AdVances in high resolution modelling and European climate Risk Assessment, https://www.primavera-h2020.eu/) are used. Although the models are quite similar in their configurations, using two models and two different horizontal resolutions allows to have a better approach to determine robust climate responses. The focus is on summer as it is the period when maximum temperatures and precipitation are highest over the peripheral Arctic regions.

2 Models and method

2.1 Models

Two fully coupled atmosphere-land-sea ice-ocean GCMs, namely, ECMWF-IFS and CNRM-CM6-1, are used in this study and described below. These models participated in the HighResMIP, which was an endorsed sub-project of the sixth phase of Coupled Model Intercomparison Project (CMIP6; Eyring et al., 2016). The model characteristics for each resolution are given in Table 1.

2.1.1 ECMWF-IFS

The atmospheric component of ECMWF-IFS, the Integrated Forecasting System (IFS), uses a semi-implicit, semi-Lagrangian discretization (Ritchie et al., 1995; Temperton et al., 2001). The model is based on the IFS cycle 43r1. The land surface component is the Hydrology Tiled ECMWF Scheme of Surface Exchanges over Land (H-TESSEL; Balsamo et al. (2009)). The ocean component is version 3.4 of the Nucleus for European Modelling of the Ocean (NEMO3.4; Madec et al., 2013). NEMO3.4 is coupled to the second version of the Louvain-la-Neuve Sea-Ice Model (LIM2; Bouillon et al. (2009); Fichefet and Morales Maqueda (1997)), which includes a three-layer model for the vertical conduction of heat in sea ice. The coupling between the ocean and atmosphere is resolved by the sequential single-executable strategy used by Mogensen et al. (2012) at

a frequency of 1 hr (Roberts et al., 2018). There is no coupling between precipitation over land and the runoff to the ocean but, to overcome this limitation, a climatological approximate calculation of the freshwater input is determined at each coastal grid point. Finally, unlike the operational setup of ECMWF where the surface energy balance is calculated in the land surface module (Mogensen et al., 2012), the skin temperature from LIM2 is coupled to mitigate the excessive sea ice volume in the Arctic.

Two different configurations of the model have been used. The first configuration, ECMWF-IFS-LR (hereafter ECMWF-LR), uses the Tco199 grid for the atmosphere, which has a horizontal resolution of about 50 km, and the ORCA1 tripolar grid for the ocean, which has a nominal resolution of $\sim 1^\circ$ (Roberts et al., 2018). The second configuration, ECMWF-IFS-HR (hereafter ECMWF-HR), uses the Tco399 grid for the atmosphere, which has a horizontal resolution of about 25 km, and the ORCA025 tripolar grid for the ocean, which has a resolution of $\sim 0.25^\circ$. The vertical resolution is the same for both configurations, with 91 levels in the atmosphere, extending up to 0.01 hPa, and 75 levels in the ocean (Madec, 2016). Beside the resolution, the only differences between the two configurations come from the resolution-dependent parameterizations in NEMO (Roberts et al., 2018). Both configurations of the model simulate reasonably well the Quasi-Biennial Oscillation (QBO) variability (not shown).

2.1.2 CNRM-CM6-1

The atmospheric component of CNRM-CM6-1 is version 6.3 of the global atmospheric model ARPEGE-Climat (Voldoire et al., 2019). It uses a semi-Lagrangian numerical integration scheme and has 91 verticals levels with a high-top level at 0.01 hPa. The model is based on cycle 37 of the ARPEGE/IFS system. This model is coupled to the surface component SURFEX, which shares the same grid and time step (Masson et al., 2013). The ocean component is NEMO3.6 (Madec et al., 2017), which includes 75 vertical levels. The sea ice component is Gelato 6 which is embedded into the ocean component. Gelato 6 uses five ice thickness categories, in which each category treats the snow as a single layer, while ice is simulated with a nine-layer vertical discretization (Voldoire et al., 2019). The coupling between the atmosphere and ocean-sea ice components is performed using the OASIS3-MCT software (Craig et al., 2017) at a 1hr frequency.

The first configuration, CNRM-CM6-1 (hereafter CNRM-LR), uses the Tl127 grid for the atmosphere, which has a nominal horizontal resolution of 130 km, and the eORCA1 horizontal grid for the ocean (Table 1), which is an extension of the ORCA1 tripolar grid that differs from ORCA1 by the use of two quasi-isotropic bipolar grids south of 67° S instead of the former Mercator grid (Voldoire et al., 2019). The second configuration, CNRM-CM6-1-HR (hereafter CNRM-HR), uses the Tl359 grid for the atmosphere, which has a nominal horizontal resolution of 50 km, and the eORCA025 horizontal grid for the ocean. The vertical resolutions are similar for both configurations and both components (atmosphere and ocean), and enable to simulate the QBO (Richter et al., 2020).

Table 1. Characteristics of the two models at two different resolutions used in this study.

	ECMWF-LR	ECMWF-HR	CNRM-LR	CNRM-HR
Atmosphere				
Model	IFS cycle 43r1		ARPEGE	
Grid name	Tco199	Tco399	Tl127	Tl359
Nominal resolution (km)	50	25	130	50
Resolution at 50°N (km)	50	25	142	50
Vertical levels	91	91	91	91
Ocean				
Model	NEMO3.4		NEMO3.6	
Grid name	ORCA1	ORCA025	eORCA1	eORCA025
Resolution	1°	0.25°	1°	0.25°
Vertical levels	75	75	75	75
Sea ice				
Model	LIM2		Gelato 6	
Ice thickness categories	1		5	

2.2 Experiments

Two different experiments are conducted with each model configuration and follow the protocol defined within the PRIMAVERA project. The first experiment, the control run (CTRL), has a constant forcing corresponding to year 1950 and is run for 100 years without including 30 years of spin-up, which are not analysed in this study. This control run is similar to the control-1950 simulation of HighResMIP (Haarsma et al., 2016). The second experiment, the perturbation run (PERT), has the same constant forcing as CTRL but with a modified sea ice albedo. In the PERT experiment, the sea ice albedo values (dry snow, melting snow, bare frozen ice and bare puddled ice) are reduced to the open ocean value (~ 0.07) from the first model time step (1st January) and are kept equal to this value through the whole model integration to achieve a large Arctic sea ice loss in summer. This perturbation increases the absorption of solar radiation and generates a melting of the snow over sea ice and of the sea ice itself. This method has already been applied in previous studies but on much longer time scales (Deser et al., 2015; Blackport and Kushner, 2016, 2017; Park et al., 2018) and produces consistent climate responses compared to other methods (Screen et al., 2018; Sun et al., 2020). The PERT experiment is run for 15 months only as our study focuses on the short-term climate response to Arctic sea ice loss. Moreover, in order to sample the internal climate variability, 40 members are performed in the PERT experiment, where each member starts from a different year of CTRL. This number of members was chosen because it allows to reach a good level of statistical significance in several high latitude regions, mainly in the surface air temperature response (Screen et al., 2014), without demanding too much computing time. One member is launched every year from CTRL

with ECMWF-LR and ECMWF-HR, every two years with CNRM-HR, and every three years with CNRM-LR. As the difference between PERT and CTRL is only a change in sea ice, comparing them enables to isolate the effect of sea ice loss. To perform our analysis, we compare each member of PERT to the member of its corresponding year in CTRL (PERT-CTRL). The atmospheric responses are scaled by the amount of Arctic sea ice extent loss averaged over the summer (July, August and September here). Finally, the statistical significance of the atmospheric response, shown in maps, has been estimated using a two-sample Kolmogorov-Smirnov test accounting for the False Discovery Rate (FDR) (Wilks, 2016). The FDR method was first described by Benjamini and Hochberg (1995) and limits spurious local test rejections. Indeed, the rejection of the null hypothesis is valid if the p values are not larger than a threshold level (10%) that depends on the distribution of the sorted p values (Wilks, 2016) obtained here thanks to a two-sample Kolmogorov-Smirnov test.

2.3 Climate extreme indices

To determine the changes in extreme climate events, twenty-seven climate extreme indices have been defined by the Expert Team on Climate Change Detection and Indices (ETCCDI) created by the World Climate Research Programme (WCRP). These indices are mainly used in historical climate model simulations (e.g., Sillmann et al., 2013a) and in model projections forced by greenhouse gas emission increases (Sillmann et al., 2013b). Eight climate extreme indices of the ETCCDI are used in this study and are summarized in Table 2. These indices are able to show extreme changes in surface air temperature and in precipitation over high latitude regions because they use either a relative change based on a percentile or a threshold suitable for these regions, such as a threshold to 0°C for the ice days index. Four indices are based on the maximum daily surface air temperature : the frequency of cold days (TX10p : % of days over the summer period when the maximum temperature is below the 10th percentile of the CTRL), the frequency of warm days (TX90p : % of days over the summer period when the maximum temperature exceeds the 90th percentile of the CTRL), the warm spell duration index (WSDI : number of days over the summer period with at least 6 consecutive days when the maximum temperature exceeds the 90th percentile of the CTRL) and the ice days (ID : number of days over the summer period when the maximum temperature remains below 0°C). This last index (ID) should not be confused with sea ice conditions. The last four indices are based on the daily precipitation : the maximum 1 day precipitation (RX1day : the maximum 1 day value of precipitation over the summer period), the wet-day precipitation (R95p : total amount of precipitation during wet days (>1mm) for days where precipitation exceeds the 95th percentile of the CTRL over the summer period), the consecutive dry days (CDD : maximum number of consecutive days over the summer period when the daily precipitation does not exceed 1mm) and the consecutive wet days (CWD : maximum number of consecutive days over the summer period when the daily precipitation exceeds 1mm). More details are given below or can be found in Zhang et al. (2011) or in Sillmann et al. (2013a) for all the indices.

For each calendar day, the values of the 10th (for TX10p) and 90th percentiles (for TX90p and WSDI) of the 40-yr period CTRL centered on a 5 day window are first calculated (the vertical blue lines in Fig. 1 on August 1st as example). For each month, the number of days exceeding the 90th percentile or less than the 10th percentile are calculated in PERT and in CTRL

and are finally weighted by the number of calendar days in this same month (divided by 31 days in August for instance). Finally, the difference between the percentage of days in a month exceeding the threshold in PERT and in CTRL is computed. The other indices are also determined for CTRL and PERT to be able to compare both simulations and to understand the effect of sea ice loss on the extremes.

Table 2. The eight climate extreme indices used in this study.

Label	**Name**	**Definition**
TX10p	Frequency of cold days	% of days over the summer period when the maximum temperature is below the 10th percentile of the CTRL
TX90p	Frequency of warm days	% of days over the summer period when the maximum temperature exceeds the 90th percentile of the CTRL
WSDI	Warm spell duration	Number of days over the summer period with at least 6 consecutive days when the maximum temperature exceeds the 90th percentile of the CTRL
ID	Ice days	Number of days over the summer period when the maximum temperature remains below 0°C
RX1day	Maximum 1 day precipitation	Maximum 1 day value of precipitation
R95p	Wet-day precipitation	Total amount of precipitation during wet days (>1mm) for days where precipitation exceeds the 95th percentile of the CTRL
CDD	Consecutive dry days	Maximum number of consecutive days when the daily precipitation does not exceed 1mm
CWD	Consecutive wet days	Maximum number of consecutive days when the daily precipitation exceeds 1mm

2.4 Studied areas

Different Arctic regions are considered according to the definitions given in Table 3 and only the continental grids of each region are used in this study. The eight climate extreme indices are first determined for each grid cell, then the regional average is computed. Note that when performing spatial averaging, the latitudinal variation in grid cell area is taken into account by weighting the values by the cosine of the latitude. There is no longitudinal variation in grid cell area.

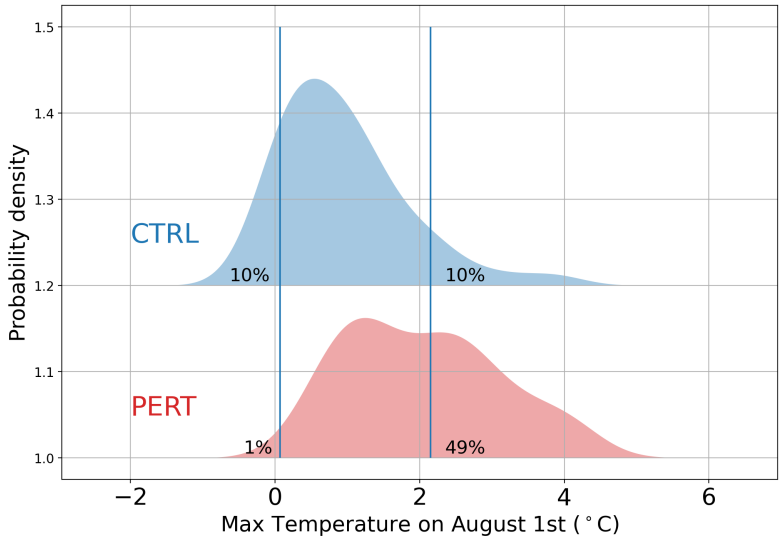

Figure 1. Probability density function of the maximum surface air temperature over Svalbard in CTRL (blue) and in PERT (red) on August 1st. The left and right vertical blue lines show the 10th and 90th percentiles of the CTRL on a 5 day window, respectively. The percentage next to the vertical lines indicates the frequency of days exceeding the 10th (left) and the 90th (right) percentiles of the CTRL.

Table 3. Latitude-longitude range of each region.

Region	Latitude	Longitude
Alaska (AL)	60° N-71° N	169° W-141° W
Northern Canada (NC)	60° N-83° N	141° W-63° W
Greenland (GR)	60° N-83° N	63° W-27° W
Iceland (IC)	63° N-67° N	25° W-12° W
Scandinavia (SC)	60° N-71° N	4°E-30° E
Svalbard (SV)	76° N-81° N	10° E-27° E
Western Russia (WR)	60° N-73° N	30° E-75° E
Eastern Russia (ER)	60° N-77° N	75° E-170° W

3 Results and discussion

3.1 Sea ice loss

The seasonality of Arctic sea ice extent in CTRL is well represented for all models with a minimum in September and a maximum in February/March (Fig. 3). However, sea ice extent is overestimated throughout the year in ECMWF-LR, while it fits well with the 1950s observations with a sea ice extent around 16 and 8 millions km^2 in March and September respectively (e.g.

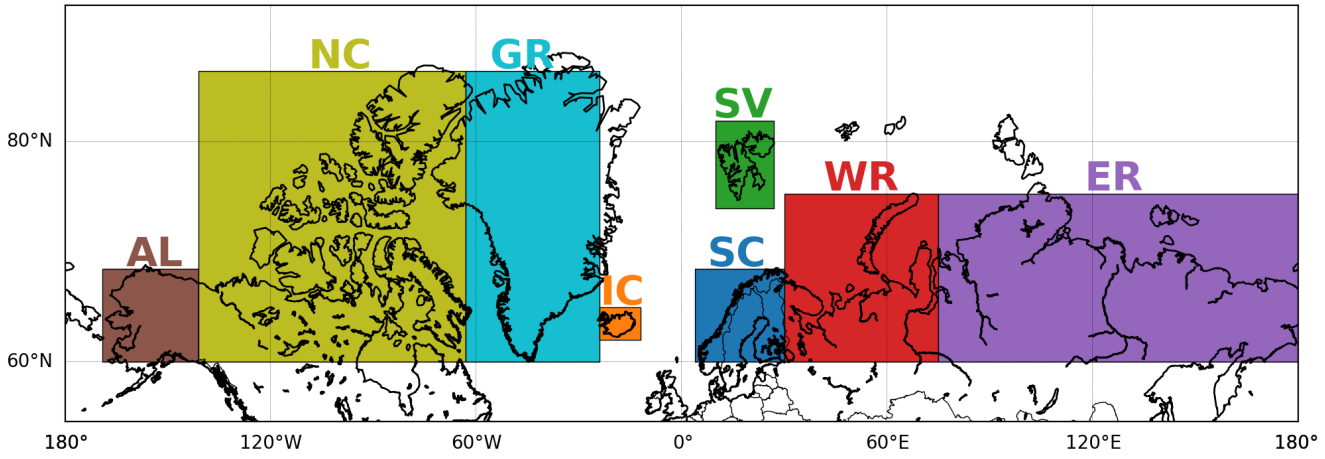

Figure 2. Regions considered in this study. AL stands for Alaska, NC for northern Canada, GR for Greenland, IC for Iceland, SC for Scandinavia, SV for Svalbard, WR for western Russia and ER for eastern Russia.

Walsh et al., 2017) in the other models. The prescribed drastic change in sea ice albedo (PERT) induces a significant reduction in Arctic sea ice extent, peaking in summer (Figs. 3 and 4). The sea ice loss in PERT is unrealistic especially in CNRM. Furthermore, using the albedo reduction technique underestimates the sea ice loss in winter, and thus impacts the magnitude of the climate responses (Sun et al., 2020). Nonetheless, a good consistency in these responses among different techniques to impose sea ice reductions has been observed (Sun et al., 2020). Moreover, the albedo reduction technique estimates well the sea ice loss during summer, the season studied here, compared to other techniques (Sun et al., 2020).

The induced sea ice loss in these experiments depends on the model used although the experimental set up is the same. The decrease in summer Arctic sea ice extent in PERT compared to CTRL reaches 30% for the two ECMWF model configurations, and is largely localized in the Barents and Kara Seas and in the eastern Arctic. In the CNRM models, it reaches up to 100% and it is associated with a total disappearance of sea ice (Figs. 3d and 4). These discrepancies may arise due to a significant difference in mean sea ice state between the models, with a large mean sea ice thickness in the ECMWF configurations (Figs. A1 and A2), which is closer to first estimates (Zhang and Rothrock, 2003) than CNRM, and relatively low ocean heat transport (Roberts et al., 2018; Docquier et al., 2019), which could lead to more sea ice being retained in PERT in ECMWF.

The sea ice loss also depends on the horizontal resolution, albeit weakly. More absolute sea ice loss is indeed simulated in the low resolution models (Fig. 3c). This might be due to larger Arctic sea ice extent in CTRL at lower resolution, particularly in the Atlantic sector of the Arctic Ocean (Figs. 3a and 4). A higher ocean resolution generally leads to a decrease in sea ice extent and volume in CTRL in several GCMs used in the PRIMAVERA project due to enhanced poleward oceanic heat

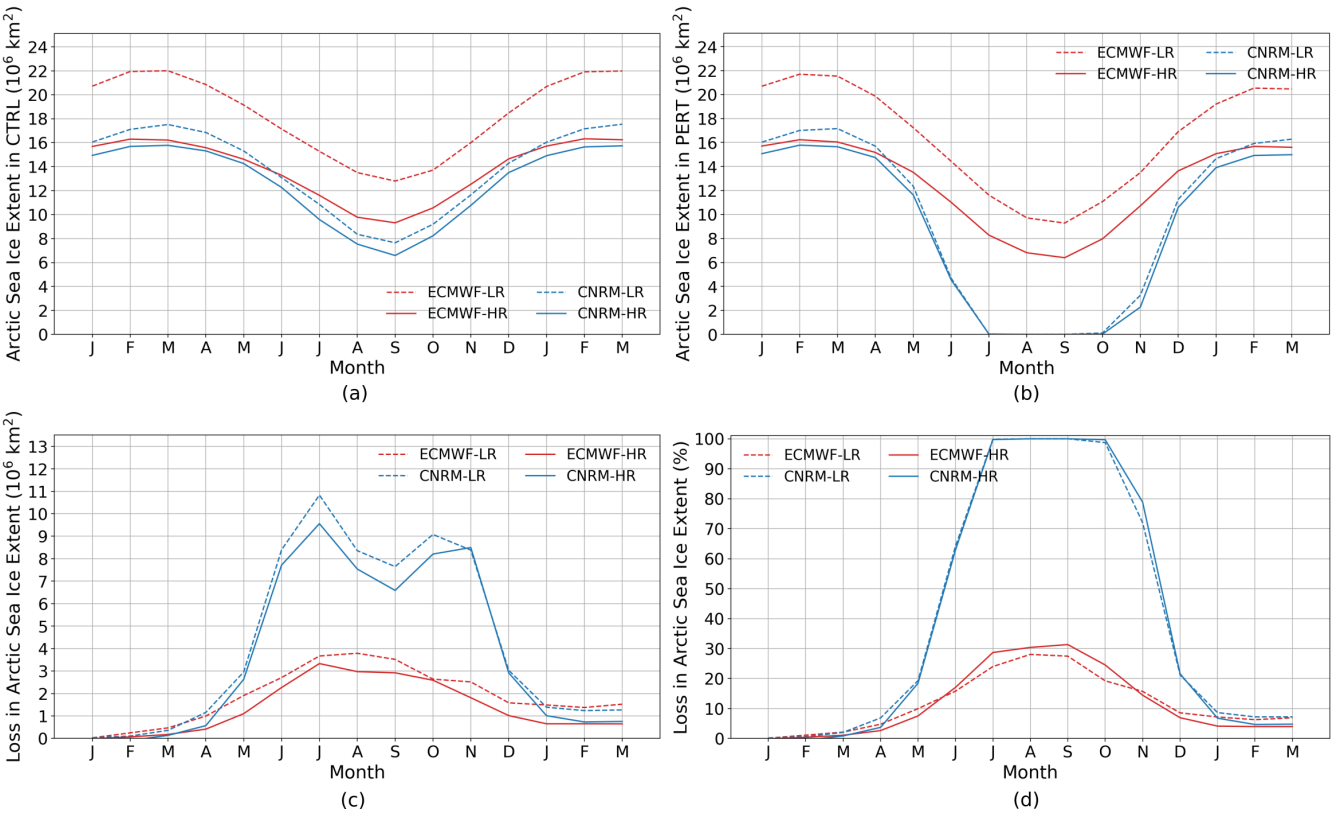

Figure 3. Arctic sea ice extent (in 10^6km^2) in CTRL (a) and in PERT (b). (c) and (d) show the decrease in Arctic sea ice extent in PERT compared to CTRL (i.e. CTRL - PERT) in 10^6km^2 and in % relative to the CTRL value, respectively.

transport (Docquier et al., 2019).

3.2 Temperature extremes

The impact of Arctic sea ice loss on the maximum surface air temperature is now analysed. Figure 5 shows the response of maximum daily surface air temperature per million km^2 of sea ice loss in summer (JAS). As expected, an increase in maximum daily temperature is found over the Arctic. The warming extends to surrounding landmasses such as Canada, Scandinavia and northern Russia. Over high latitudes, the CNRM response is larger than the ECMWF one, even after scaling the response by the amount of sea ice loss. This could be explained by the insulating effect of sea ice in ECMWF, which still simulates more than 2m-thick sea ice in PERT in summer (Fig. A1b), and can limit the warming in that model. The change in horizontal resolution does not strongly impact the response, as observed in Streffing et al. (2021), except over the southern Labrador Sea in ECMWF. In this model, sea ice is present in that area in CTRL at low resolution but not at high resolution, leading to a

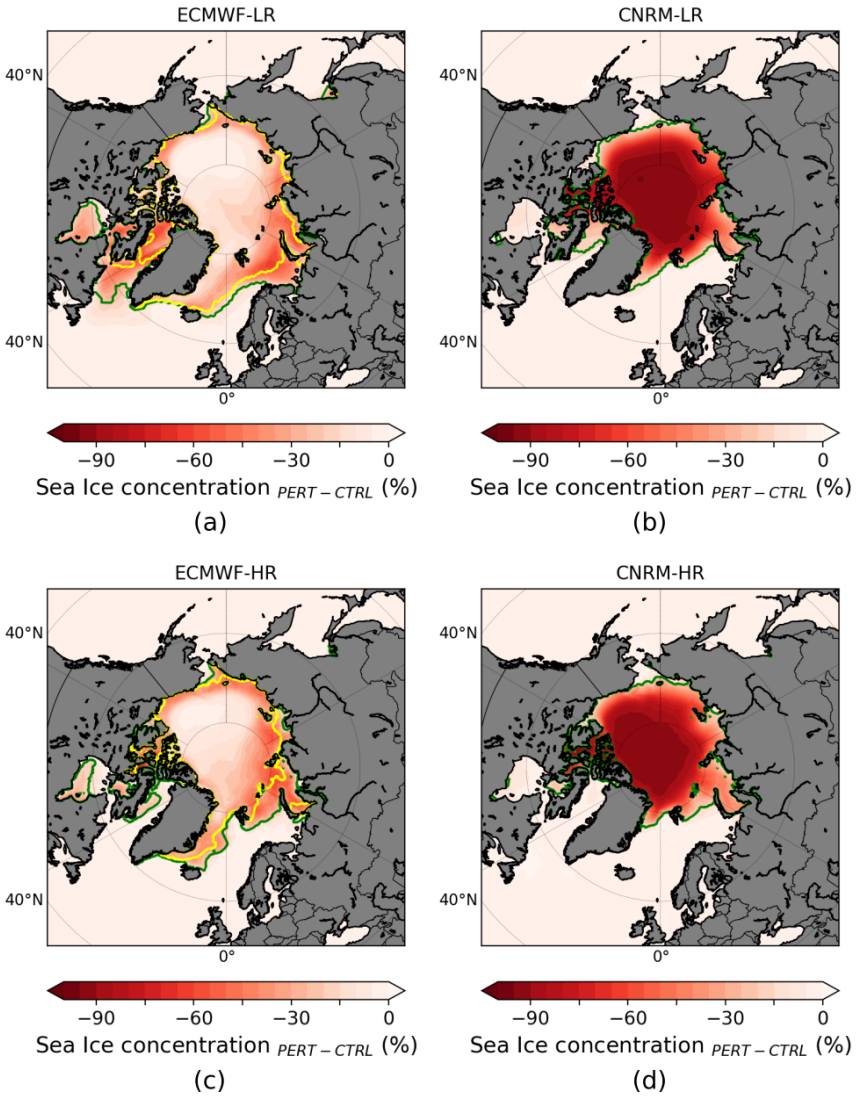

Figure 4. Arctic sea ice concentration change (PERT-CTRL) in summer (JAS) in ECMWF-LR (a) and CNRM-LR (b). (c-d) as (a-b) but for models at high resolution. The green and yellow lines show the sea ice edge (15% ice concentration) from CTRL and PERT, respectively. Note that for the two CNRM model configurations, no yellow line is present because the sea ice has disappeared in PERT.

warming in ECMWF-LR that is nearly absent in ECMWF-HR.

The probability density function (PDF) of the daily summer maximum temperature is shown in Fig. 6 for eight different peripheral Arctic regions (defined in Table 3 and Fig. 2). The change in PERT compared to CTRL is stronger in CNRM (Fig. 6) because the response cannot be scaled by the amount of sea ice loss in this figure and CNRM experiences a larger Arctic sea ice loss than ECMWF (Figs. 3 and 4). A shift to the right of the PDF in PERT compared to CTRL, going hand in hand

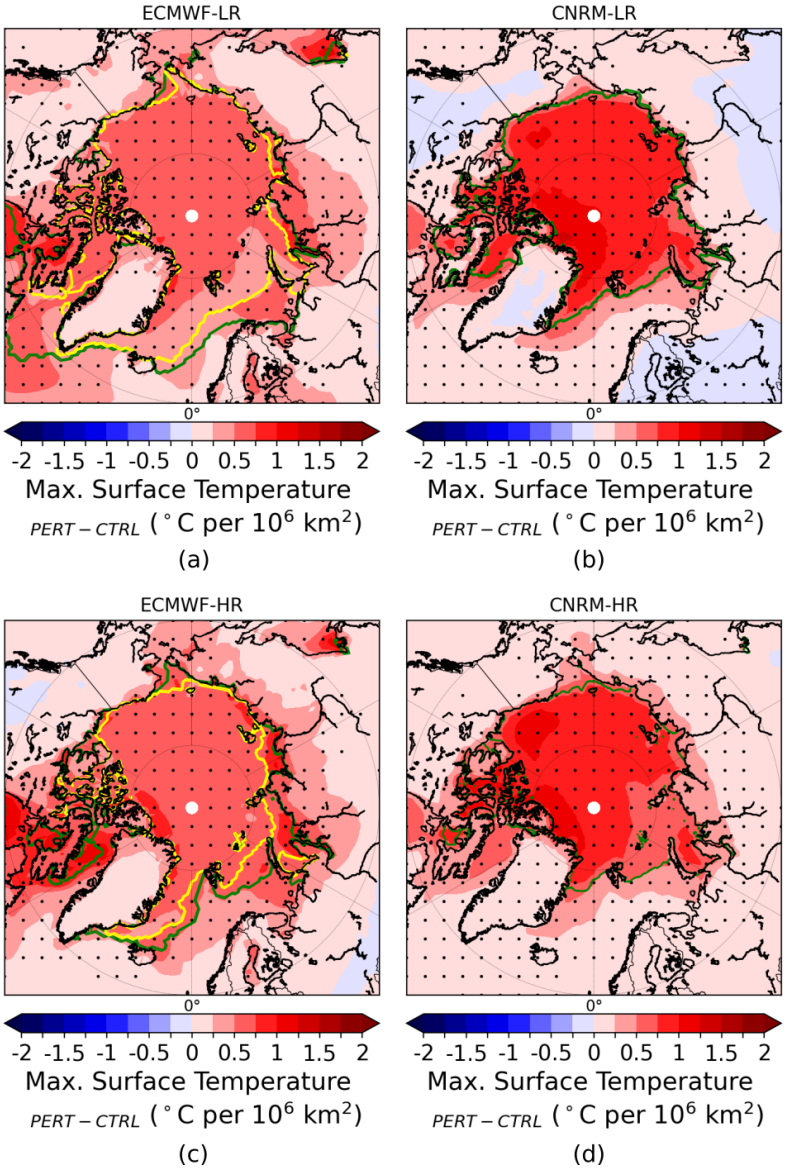

Figure 5. Ensemble mean changes (PERT-CTRL) in maximum daily surface air temperature response over the entire summer (JAS) scaled by the amount of sea ice extent loss for ECWMF-LR (a), CNRM-LR (b), ECMWF-HR (c) and CNRM-HR (d). The dots show where the response is statistically significant according to a 10% level FDR test associated with a Kolmogorov-Smirnov test. The green and yellow lines represent the sea ice edge (15% ice concentration) from CTRL and PERT, respectively.

with a shift of the mean towards higher values, occurs due to sea ice loss over all the selected regions. Nonetheless, this shift is not symmetrical for most regions, with a larger shift of the left part of the distribution (low temperatures) compared to the right part (high temperatures) leading to a change in the shape of the distribution. This means that low maximum surface air

temperatures increase more than high maximum surface air temperatures, in agreement with previous studies focusing on high latitudes (Kharin et al., 2013; Sillmann et al., 2013a).

Furthermore, the magnitude of the warming depends on the region. The warming over Svalbard is obviously stronger than in other regions as Svalbard is made up of islands surrounded (at least in part) by sea ice in early summer in all models in CTRL. Thus, the sea ice loss in PERT impacts more easily this region than a continent or an island further south such as Iceland. Northern Canada, which is composed of hundred of islands surrounded by sea ice, is the region with the second strongest warming. Greenland, although it is an island partially surrounded by sea ice, experiences less warming than the two last regions because an ice sheet covers almost the whole island and temperatures are much lower over central Greenland, where the altitude is high, than over other Arctic regions, which does not lead to an important melt of the sea ice and could mitigate the maximum surface air temperature response to a sudden sea ice loss over that region (Figs. 5 and 6). The warming over Greenland and North Canada can be related to a negative change of the North Atlantic Oscillation (NAO) (Folland et al., 2009; Ding et al., 2014). However, in these experiments, only CNRM-LR displays a negative change in the NAO but this change is small compared to the variability of the ensemble (Fig. A3). As this index exhibits a high variability, 40 members (and even 80 members by combining the two resolutions) are not enough to detect a robust response in the NAO index.

The increase in maximum surface air temperature over the peripheral Arctic regions is robust although a large internal climate variability is present. The signal to noise ratio, estimated as the ensemble mean response divided by the standard error, reveals that the signal exceeds the noise due to internal climate variability over the vast majority of high-latitude regions (Fig. 7a). However, in some regions such as western Scandinavia, the center of Greenland, the northwest territories of Canada and the regions of Russia close to 60° N, the noise exceeds the signal showing that the response is small compared to the role of internal climate variability even in regions relatively close to the sea ice front.

Figure 8 shows four different temperature extreme indices (see Sect. 2.3) for the eight different regions in summer. As expected, all regions experience an increase in frequency of warm days (Fig. 8a), a decrease in frequency of cold days (Fig. 8b), an increase of warm spell duration (Fig. 8c) and a decrease of the number of ice days (Fig. 8d) due to Arctic sea ice loss. Svalbard exhibits a more drastic change compared to other regions. Indeed, an absolute increase of around 5% (up to 8% in CNRM-LR) in warm days frequency (Fig. 8a) and also of around 1 day per month (up to 2,5 days per month in CNRM-LR) in warm spell duration (Fig. 8c) per million km^2 of sea ice loss are simulated over this region. Furthermore, a loss of one million km^2 of sea ice leads to a reduction of at least one ice day per month in Svalbard (Fig. 8d). Other regions experience less intense change in frequency or persistence but all models agree on the sign of the change except over Scandinavia. These results cannot be directly compared to those of the idealized atmospheric general circulation model simulations forced by projected Arctic sea ice loss of Screen et al. (2015) because, in the latter study, the response is not scaled by the amount of sea ice loss, the oceanic areas are taken into account and the response is averaged over an entire year. However, a global Arctic sea ice loss does not seem to lead to the recent increase of hot waves that happened almost only over Northeastern Canada and Greenland

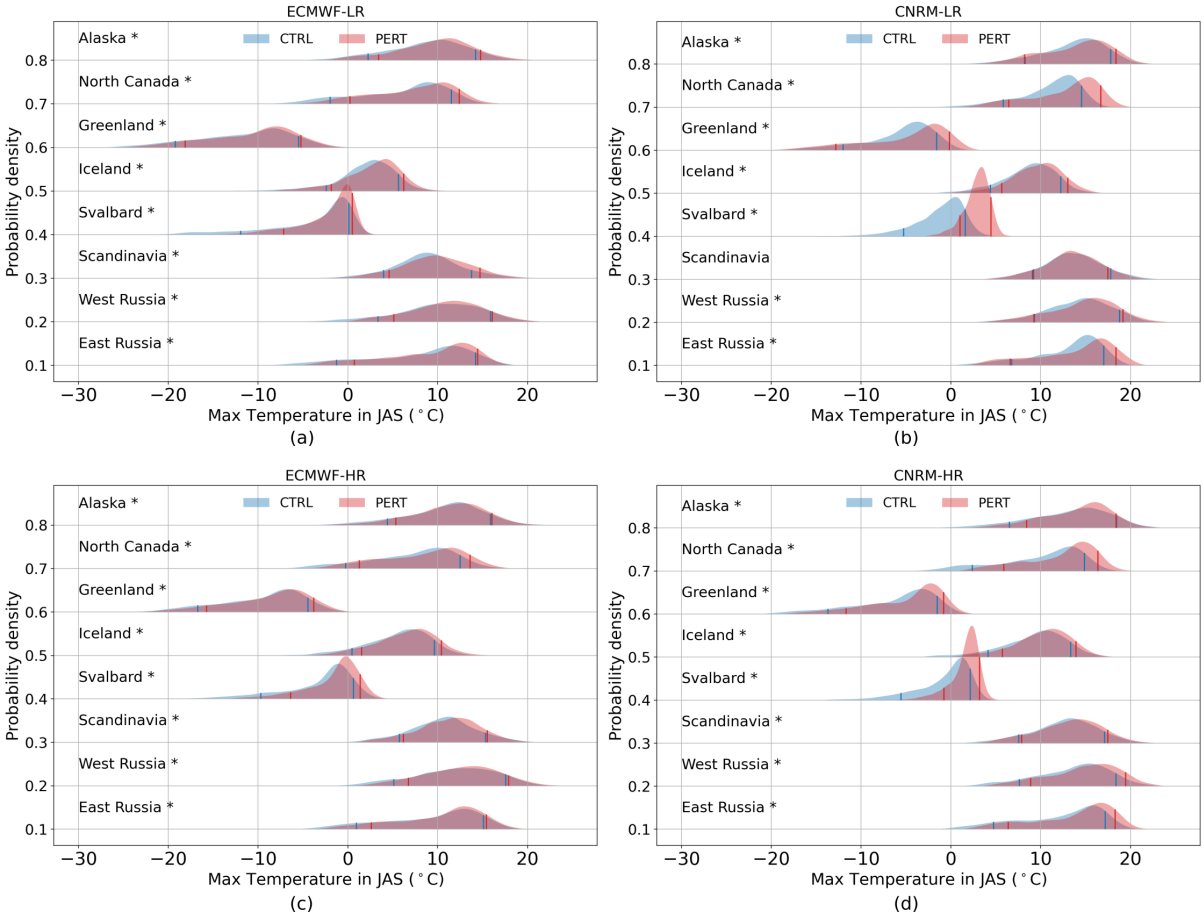

Figure 6. Probability Density Function (PDF) of the daily maximum surface air temperature ($^\circ\ C^{-1}$) in summer (JAS) for ECWMF-LR (a), CNRM-LR (b), ECMWF-HR (c) and CNRM-HR (d). PDF of the CTRL is the blue distribution and PDF of the PERT is the red distribution. The left blue (red) line and the right blue (red) line correspond to the 10th percentile and 90th percentile of the CTRL (PERT), respectively. A star next to the name of the region shows if the distribution change is statistically significant according to a 5% level Kolmogorov-Smirnov test. An offset in Y-axis of 0.1 is taken into account for each region.

(Dobricic et al., 2020).

The maximum daily surface air temperature increase is larger in autumn than in summer (not shown), even if the sea ice loss is smaller in autumn (see Fig. 3). This can be explained by the turbulent heat flux response, which is enhanced in autumn due to a large contrast between the air and surface temperatures during this season (e.g. Deser et al., 2010). However, the increase in frequency of warm days and in the warm spell duration are larger in summer over peripheral Arctic regions (not shown), highlighting the usefulness of studying the response of extreme events during this season. Finally, all extreme indices studied here show a significant increase mainly localized over the Arctic Ocean, which hardly extends over continents (e.g. Fig. A4).

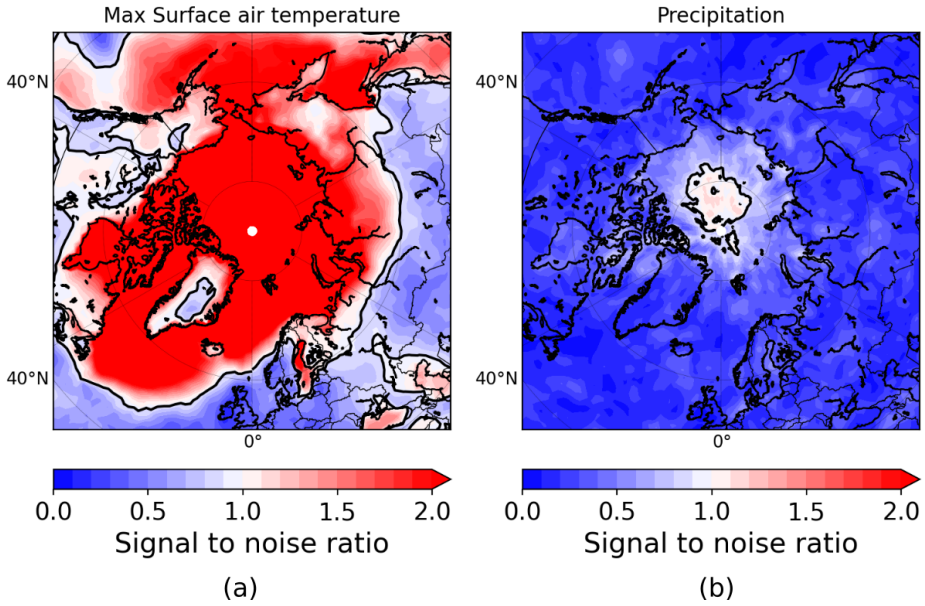

Figure 7. Signal to noise ratio in summer averaged for all the models for the daily maximum surface air temperature (a) and for the daily precipitation (b) responses to summer Arctic sea ice loss. The black line represents where the signal to noise ration is equal to 1.

Nonetheless, the change in frequency of extremes (warm days and cold days) extends more easily towards continents than the change in persistence of extremes (WSDI).

3.3 Precipitation extremes

We now investigate the precipitation response with Fig. 9, which shows the monthly mean precipitation response to sea ice loss in summer. An increase in precipitation is found over the Arctic, which is only statistically significant in CNRM. Newly-open waters lead to an increase in evaporation, resulting in enhanced precipitation there, in agreement with previous studies (e.g. Deser et al., 2010; Semmler et al., 2012; Bintanja and Selten, 2014; Semmler et al., 2016; Smith et al., 2017; England et al., 2018). However, although little sea ice melts in PERT over Central Arctic in summer in ECMWF, an increase in precipitation, not statistically significant, is simulated over this region (Fig. 9a,c). This shows the small signal and the greater importance of internal climate variability for this variable compared to surface air temperature (Screen et al., 2014). Indeed, only the region close to the North Pole experiences a signal larger than the noise for the precipitation response (Fig. 7b), elsewhere, the response is weak compared to internal variability. Furthermore, even by combining the two resolutions (and having 80 members), the precipitation response is still not statistically significant in peripheral Arctic regions (not shown).

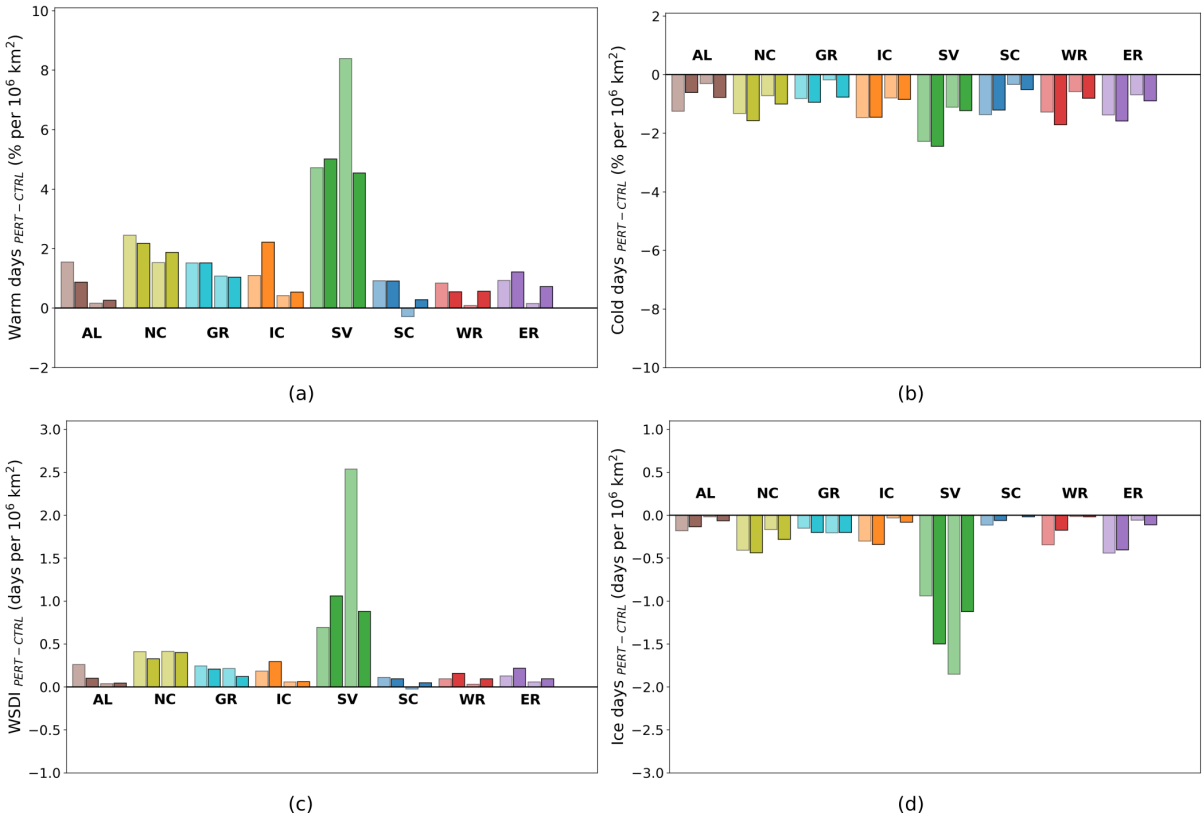

Figure 8. Ensemble mean changes (PERT-CTRL) per month averaged in summer (JAS) in warm days (a), cold days (b), warm spell duration index (c) and ice days (d) scaled by the amount of sea ice extent loss for the eight regions defined in Table 3 (Fig. 2) for ECMWF-LR (left light bar), ECMWF-HR (left dark bar), CNRM-LR (right light bar) and CNRM-HR (right dark bar).

No significant change in net precipitation (P-E) is observed over Central Arctic (Fig. A5) showing that the increase in precipation is balanced by the increase in local evaporation over that region. However, a decrease in P-E is detected near the continental edges of the Arctic Ocean, which is statistically significant in CNRM (Fig. A5b,d). This highlights the fact that the increase in evaporation is larger than the increase in precipitation, which leads to an increase in ocean surface salinity (not shown) despite the melting sea ice in these areas.

The PDF of the daily precipitation in summer is shown in Fig. 10. A shift to the right of the PDF in PERT, reflecting an increase in precipitation, occurs in some regions due to sea ice loss. Nonetheless, the shift is weaker in the daily precipitation response (Fig. 10) than in the daily maximum surface air temperature response (Fig. 6). The change in the distribution between CTRL and PERT seems to be symmetrical in all regions except in Svalbard in CNRM. As for the maximum surface air temperature (Fig. 6), the shift is larger in CNRM due to the greater loss of sea ice (Fig. 10) leading to a greater surface heat flux change in this model than in ECMWF (not shown), and can explain the larger response in precipitation in CNRM. Moreover,

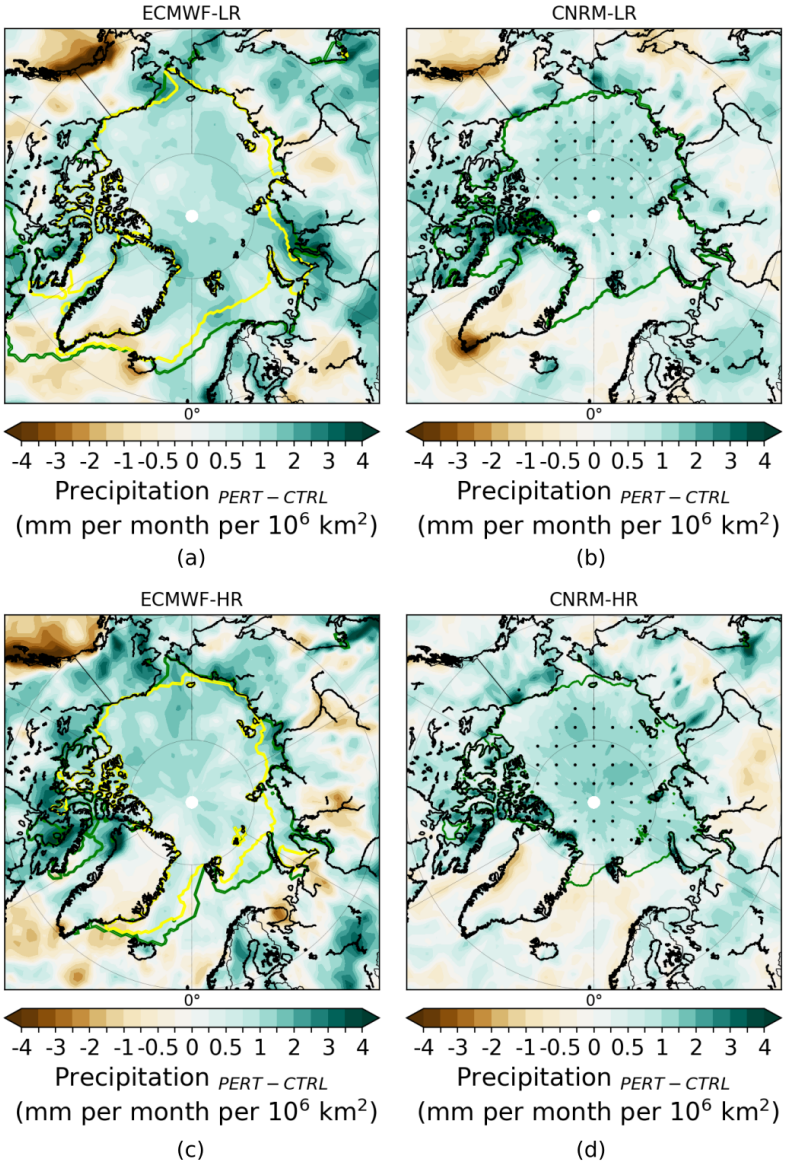

Figure 9. Ensemble mean changes (PERT-CTRL) in summer (JAS) precipitation scaled by the amount of sea ice extent loss for ECWMF-LR (a), CNRM-LR (b), ECMWF-HR (c) and CNRM-HR (d). The dots show where the response is statistically significant according to a 10% level FDR test associated with a Kolmogorov-Smirnov test. The green and yellows lines represent the sea ice edge (15% ice concentration) from CTRL and PERT, respectively.

the increase in precipitation is also stronger in Svalbard and in northern Canada because these regions are made up of islands surronded by sea ice, which melts in PERT. Newly-open waters are observed in these regions and lead to a significant increase in precipitation. Furthermore, surface waters are warmer in PERT and generate more evaporation. Finally, as the surface air

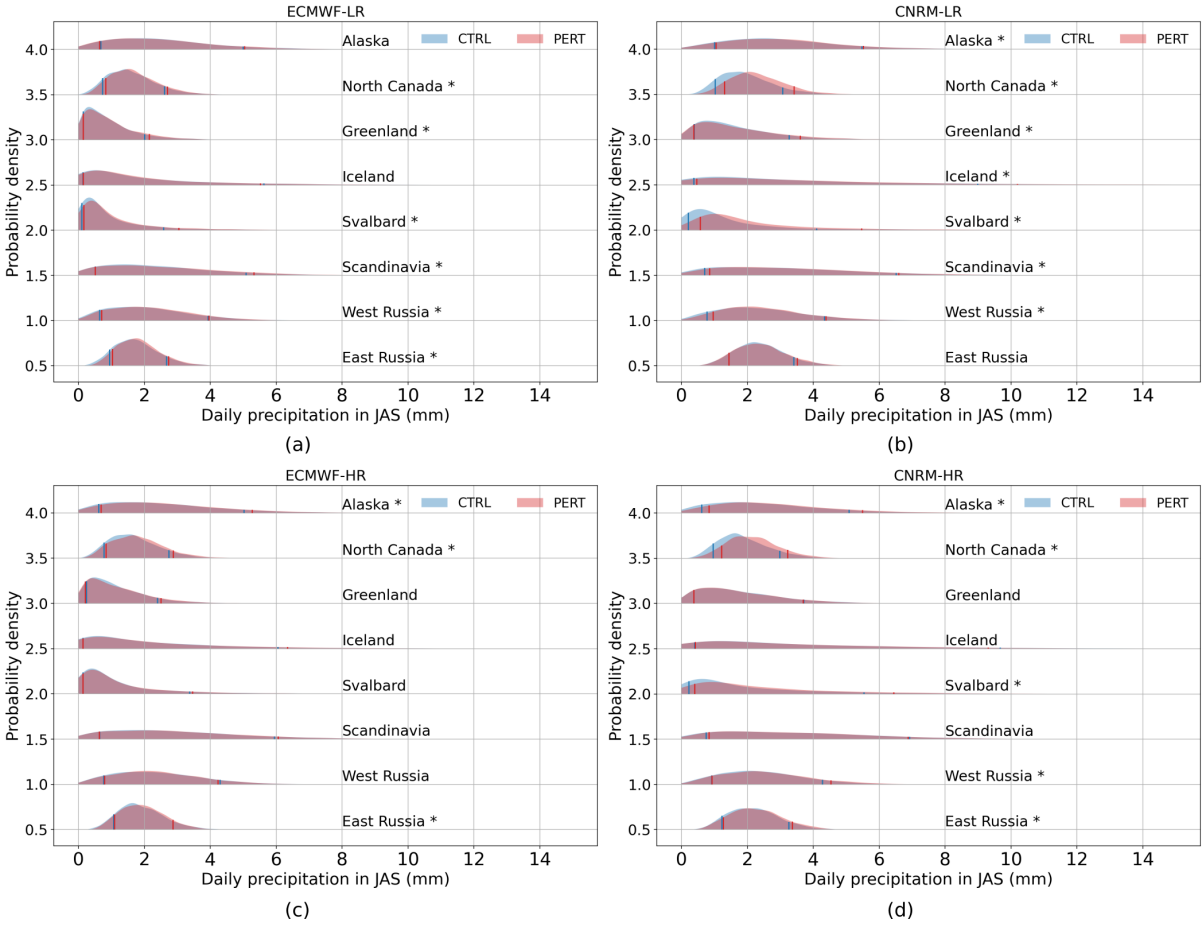

Figure 10. PDF of the daily precipitation in summer (JAS) for ECWMF-LR (a), CNRM-LR (b), ECMWF-HR (c) and CNRM-HR (d). PDF of the CTRL is the blue distribution and PDF of the PERT is the red distribution. The left blue (red) line and the right blue (red) line correspond to the 10th percentile and 90th percentile of the CTRL (PERT), respectively. A star next to the name of the region shows if the distribution change is statistically significant according to a 5% level Kolmogorov-Smirnov test. An offset in Y-axis of 0.1 is taken into account for each region.

temperature increases in PERT, the water vapor content increases and can therefore potentially generates more precipitation. In all other regions, the shift to the right of the precipitation distribution is rather weak (Fig. 10). If we now compare the resolutions, no significant differences occur between the LR and the HR, as reported in Streffing et al. (2021).

Figure 11 shows four different precipitation extreme indices (see Sect. 2.3) for the regions in the peripheral Arctic in summer. An increase in the intensity of precipitation extreme is simulated in all regions (Fig. 11a,b) and supports the recent observed (Chernokulsky et al., 2019) and projected (Kharin et al., 2018) increase in heavy precipitation. If we average all the models, Svalbard is still the region with the largest increase in intensity of precipitation (Fig. 11a,b). However, other regions further

south, such as Iceland or Scandinavia, experience an increase in intensity which can be larger than in Svalbard in some models when the very wet days in a month are summed up (Fig. 11b). Regions over Russia display less significant changes, mainly in the maximum 1 day precipitation indice (Fig. 11a).

The change in persistence of extreme precipitation over the different regions (Fig. 11c,d), mainly in consecutive dry days (Fig. 11c), is not as consistent as the change in magnitude (Fig. 11a,b). Several regions, such as Greenland, Iceland, Scandinavia and western Russia, have a different sign in the response in the consecutive dry days duration to sea ice loss (Fig. 11c). In the other regions, all models show a decrease in the number of consecutive dry days. Nonetheless, the change in consecutive wet days duration is more consistent among the regions and the models (Fig. 11d). Over Greenland, a larger change in magnitude than in persistence of extreme precipitation is simulated and could be related to the lack of a significant circulation change (e.g. Fig. A3). Over Svalbard, a decrease in consecutive dry days duration and an increase in consecutive wet days duration of up to 0.3 days per million km^2 of sea ice loss is modelled in CNRM-LR (Fig. 11c,d), but is weaker in the other models. Finally, the response in persistence of extreme precipitation remains more restricted to the Arctic Ocean (Fig. 12) than the response in monthly mean precipitation (Fig. 9).

4 Conclusions

As the Arctic sea ice continues its decline throughout the century, its variability is projected to increase (e.g. Goosse et al., 2009). Observing a drastic summer sea ice retreat for one particular year becomes a distinct possibility, yet the consequences of such an event on the atmosphere have been little explored. The summertime changes in temperature and precipitation extremes over the peripheral Arctic regions after a sudden sea ice retreat was investigated here. To our knowledge, this study is the first one to address this last question in depth following a coordinated (fully coupled) two-model approach in which idealized albedo experiments have been conducted. These experiments help to isolate as much as possible the effect of the Arctic sea ice loss without confounding factors, such as a change in sea surface temperature or in radiative forcing.

During the summer with a strong decline in Arctic sea ice extent, an increase in frequency and persistence of the maximum surface air temperature occurs over all the peripheral Arctic regions. This increase is especially large in regions made up of islands surronded by sea ice in CTRL such as Svalbard or the northern Canada. Svalbard experiences the largest change with an increase of more than 4% (per million km^2 of sea ice loss) in the frequency of warm days and of around 1 day (per million km^2 of sea ice loss) in warm spell duration index. Over all regions, the low maximum temperatures increase more than the high maximum temperatures in summer in response to sea ice loss.

An increase in extreme precipitation is also found over the peripheral Arctic regions. Nonetheless, the change in precipitation is smaller and less significant than the change in maximum surface air temperature. Furthermore, the response in extreme

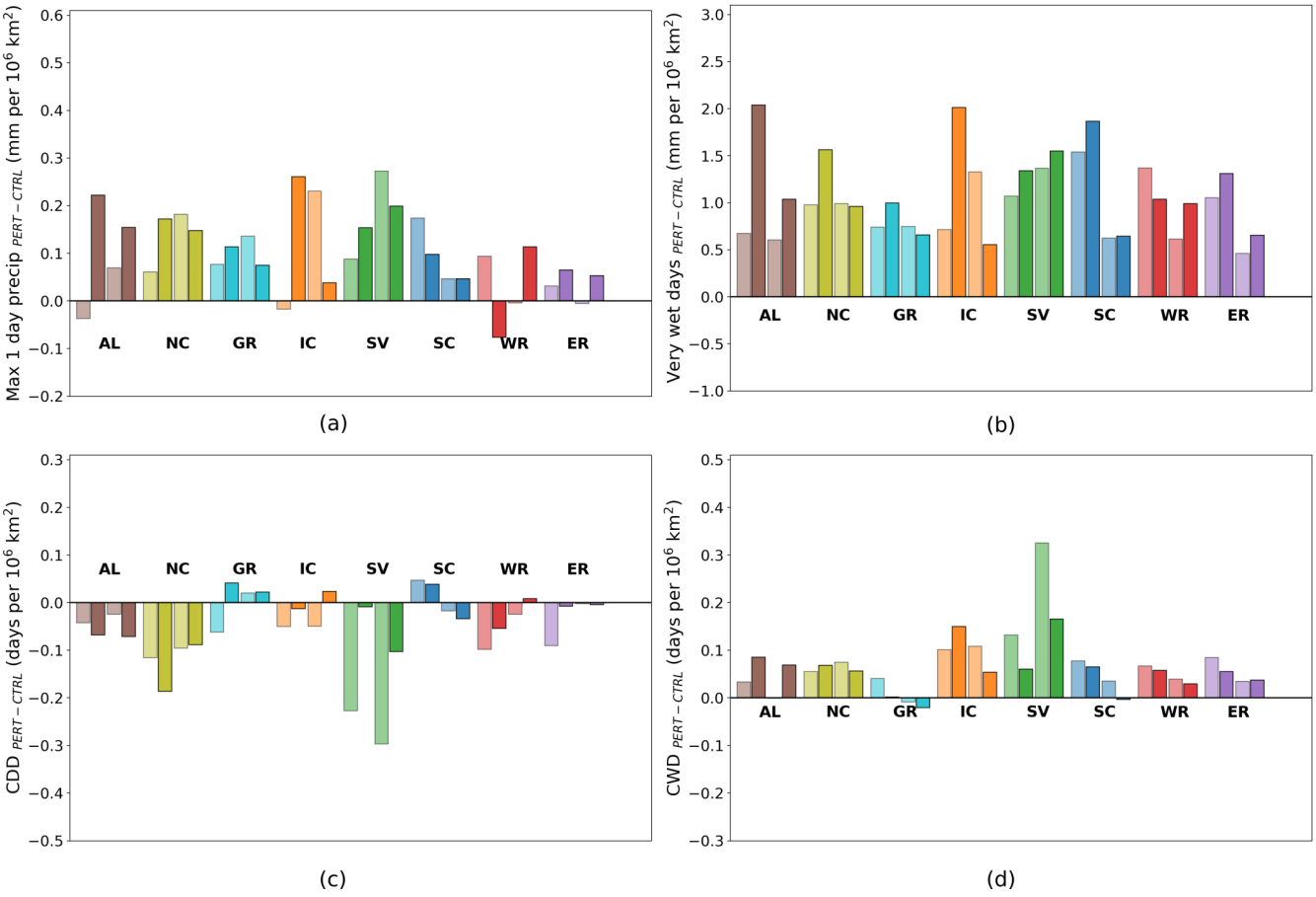

Figure 11. Ensemble mean changes (PERT-CTRL) per month in summer (JAS) in maximum one day precipitation (a), very wet days (b), consecutive dry days (c) and consecutive wet days (d) scaled by the amount of sea ice extent loss for the eight regions (Fig. 2) for ECMWF-LR (left light bar), ECMWF-HR (left dark bar), CNRM-LR (right light bar) and CNRM-HR (right dark bar). The response is scaled by the amount of the summer Arctic sea ice loss.

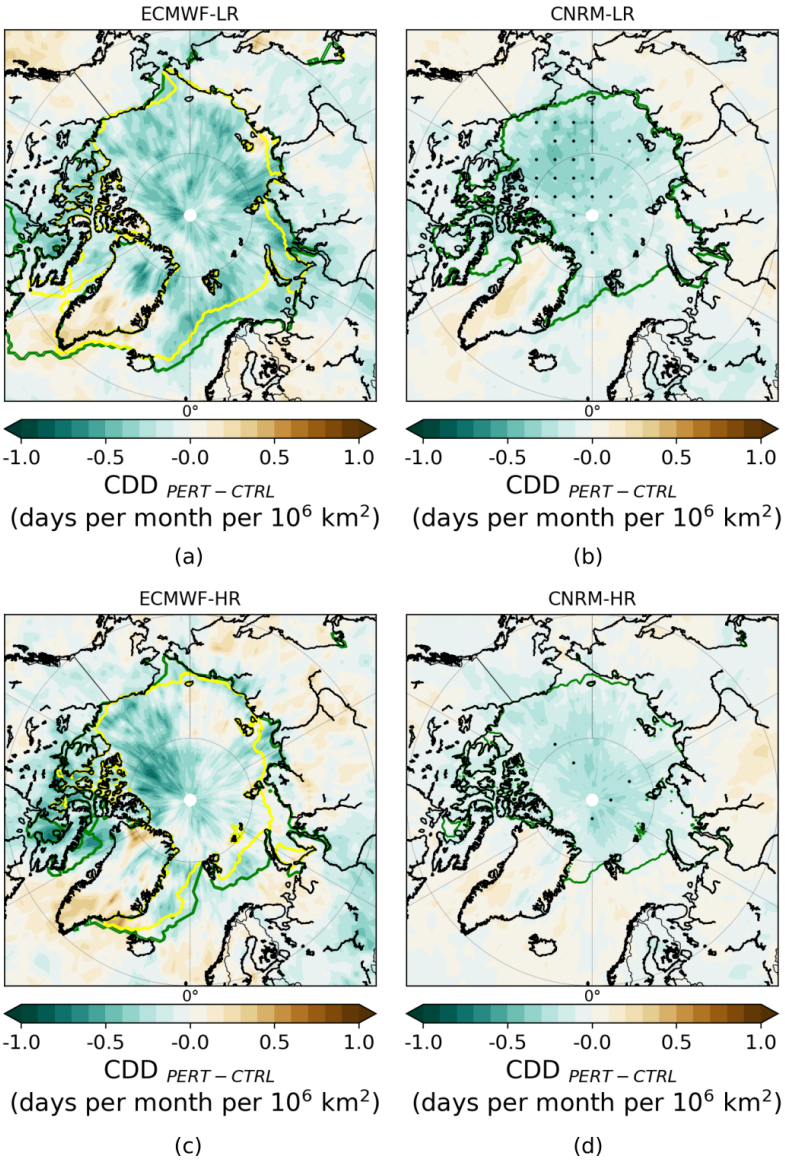

Figure 12. Ensemble mean changes (PERT-CTRL) in summer (JAS) consecutive dry days duration scaled by the amount of sea ice extent loss in ECWMF-LR (a), CNRM-LR (b), ECMWF-HR (c) and CNRM-HR (d). The dots show where the response is statistically significant according to a 10% level FDR test associated with a Kolmogorov-Smirnov test. The green and yellow lines represent the sea ice edge (15% ice concentration) for CTRL and PERT, respectively.

precipitation remains more restricted to the Arctic Ocean than the response in mean precipitation. Consistent with the temperature response, Svalbard shows again the largest change, with a decrease in consecutive dry days duration and an increase in consecutive wet days duration of 0.3 days (per million km^2 of sea ice loss) in CNRM-LR. However, an increase in the magnitude of precipitation occurs in all the peripheral Arctic regions in all models.

The increase in extreme precipitation is found in all the peripheral regions but is relatively small compared to internal climate variability. For the maximum surface air temperature, the signal exceeds the noise in the majority of the regions north of 60° N. Even if the two models (ECMWF and CNRM) experience different Arctic sea ice loss, both show a change (scaled by the amount of sea ice loss) relatively similar in maximum surface air temperature and precipitation, suggesting that the response over the peripheral Arctic regions evolves about linearly with respect to the amount of sea ice loss. This shows the minor importance of the role of the dynamical response in high latitudes, which tends to be non-linear (Petoukhov and Semenov, 2010), compared to the role of the thermodynamical response in summer. However, a stronger sea ice loss could produce a larger statistically significant response even when the response is scaled by the amount of sea ice loss. Finally, using a higher horizontal resolution does not considerably affect the response on extreme maximum surface temperature or precipitation.

Further studies are encouraged to study the response of climate extremes over Arctic regions to sudden sea ice loss as it can influence local communities (Ford et al., 2008), agriculture (Stevenson et al., 2014) and biodiversity (Hollowed et al., 2013; Haug et al., 2017). More members would be needed to detect robust change in extreme precipitation even at high latitudes. Moreover, it would be interesting to analyse the change in extremes over peripheral Arctic regions in summer with other sensitivity experiments simulating a more realistic seasonal cycle of Arctic sea ice loss and using different sea ice perturbation techniques, such as nudging. In conclusion, it is clear that Arctic sea ice loss alone impacts the extreme events on maximum surface temperature over the peripheral Arctic regions, and efforts such as those previously mentioned would help better quantify these climate impacts on these regions.

Appendix A

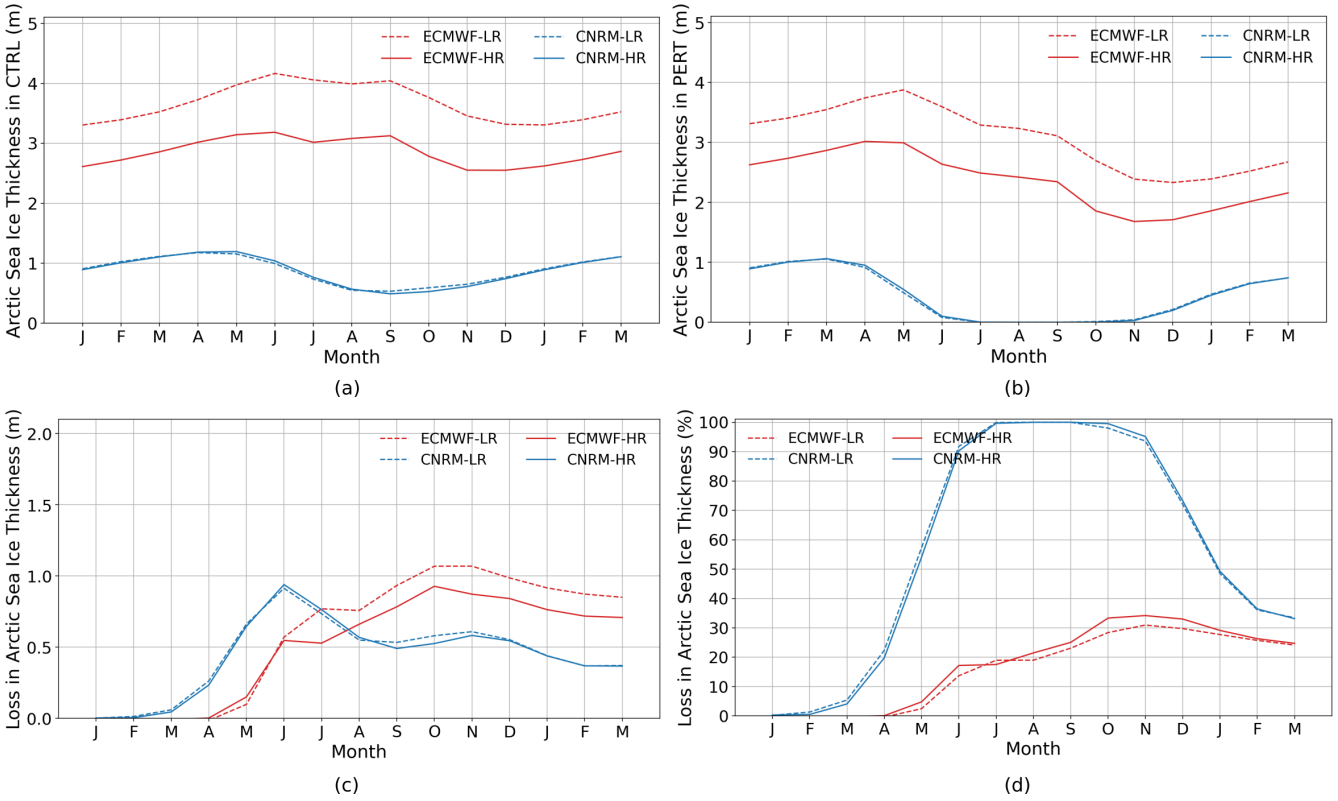

Figure A1. Arctic sea ice thickness (in m) in CTRL (a) and in PERT (b). (c) and (d) show the decrease in Arctic sea ice extent in PERT compared to CTRL (i.e. CTRL - PERT) in m and in % relative to the CTRL value, respectively.

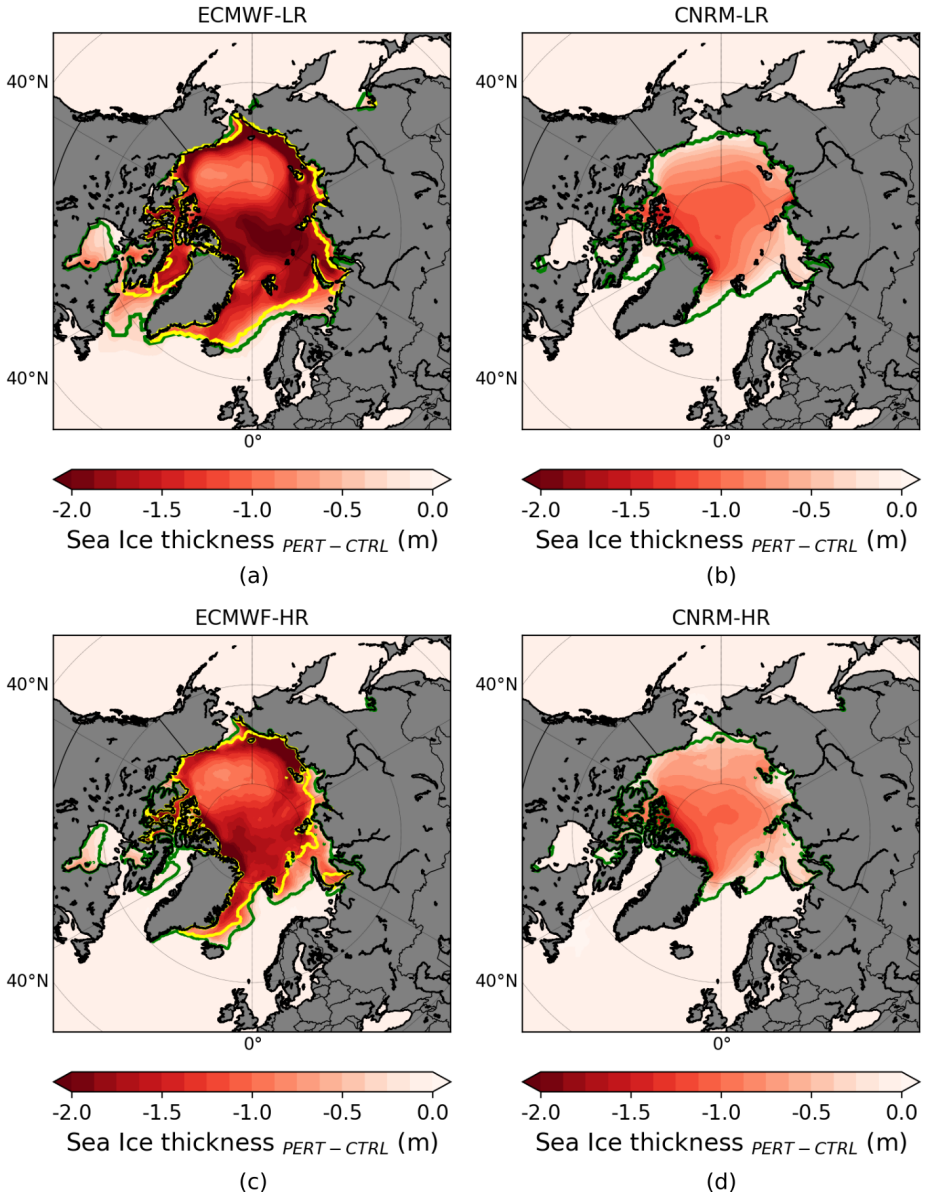

Figure A2. Arctic sea ice thickness change (PERT-CTRL) in summer (JAS) in ECMWF-LR (a) and CNRM-LR (b). (c-d) as (a-b) but for models at high resolution. The green and yellow lines show the sea ice edge (15% ice concentration) from CTRL and PERT, respectively. Note that for the two CNRM model configurations, no yellow line is present because the sea ice has disappeared in PERT.

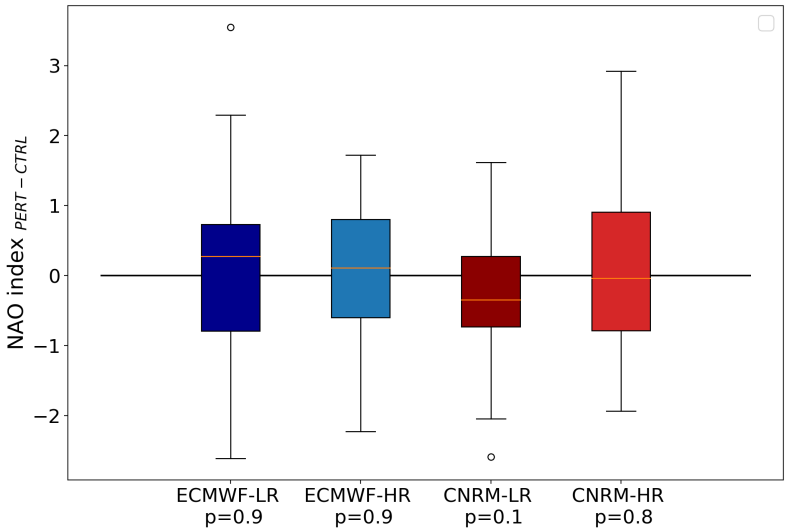

Figure A3. Boxplot of the summer NAO index (station-based method) in PERT compared to CTRL, where the CTRL has been taken as the 40 year reference period, for all members in each model. The p-value of a Kolmogorov-Smirnov test between PERT and CTRL is shown below each boxplot.

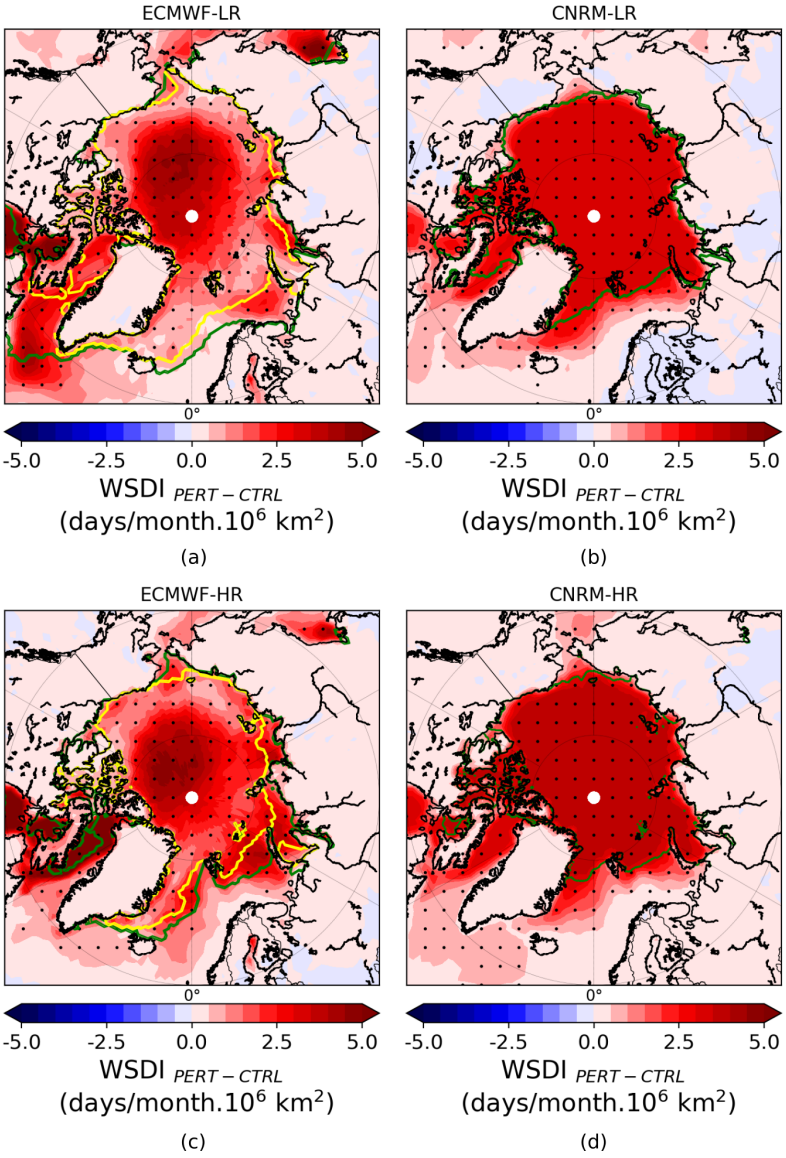

Figure A4. Ensemble mean changes (PERT-CTRL) in summer (JAS) warm spell duration index scaled by the amount of sea ice extent loss in ECWMF-LR (a), CNRM-LR (b), ECMWF-HR (c) and CNRM-HR (d). The dots show where the response is statistically significant according to a 10% level FDR test associated with a Kolmogorov-Smirnov test. The green and yellow lines represent the sea ice edge (15% ice concentration) from CTRL and PERT, respectively.

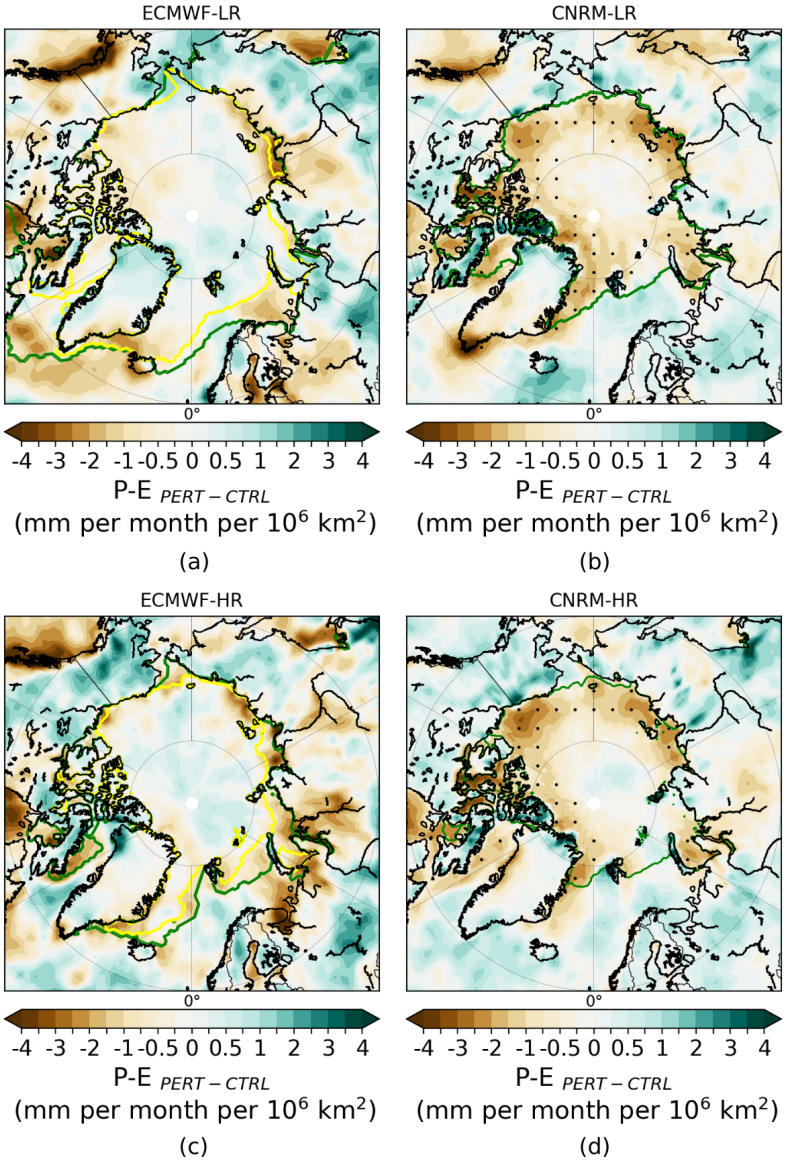

Figure A5. Ensemble mean changes (PERT-CTRL) in summer (JAS) precipitation minus evaporation (P-E) scaled by the amount of sea ice extent loss for ECWMF-LR (a), CNRM-LR (b), ECMWF-HR (c) and CNRM-HR (d). The dots show where the response is statistically significant according to a 10% level FDR test associated with a Kolmogorov-Smirnov test. The green and yellows lines represent the sea ice edge (15% ice concentration) from CTRL and PERT, respectively.

Author contributions. SD, TF, FM, RM conceptualized the science plan. RM, SC, CR, SK and RS conducted the experiments. SD performed the analyses, produced the figures and wrote the manuscript based on the insights from the co-authors.

Competing interests. The authors declare that they have no conflict of interest.

Acknowledgements. Steve Delhaye is F.R.S–FNRS research fellow, Belgium (grant no. 1.A119.20). François Massonnet is a F.R.S.-FNRS Research Associate. Computational resources have been provided by the supercomputing facilities of the Université catholique de Louvain (CISM/UCL) and the Consortium des Équipements de Calcul Intensif en Fédération Wallonie Bruxelles (CÉCI) funded by the Fond de la Recherche Scientifique de Belgique (F.R.S.–FNRS) under convention 2.5020.11. The research leading to these results has received funding from the European Commission's Horizon 2020 PRIMAVERA (GA 641727) project.

Data availability. The data from the ECMWF model can be accessed using www.jasmin.ac.uk via https://prima-dm1.jasmin.ac.uk. The data from the CNRM model are openly available and can be shared upon request.

References

Balsamo, G., Beljaars, A., Scipal, K., Viterbo, P., van den Hurk, B., Hirschi, M., and Betts, A. K.: A Revised Hydrology for the ECMWF Model: Verification from Field Site to Terrestrial Water Storage and Impact in the Integrated Forecast System, Journal of Hydrometeorology, 10, 623–643, https://doi.org/10.1175/2008JHM1068.1, 2009.

Barnes, E. A. and Screen, J. A.: The impact of Arctic warming on the midlatitude jet-stream: Can it? Has it? Will it?, Wiley Interdisciplinary Reviews: Climate Change, 6, 277–286, https://doi.org/10.1002/wcc.337, 2015.

Benjamini, Y. and Hochberg, Y.: Controlling the false discovery rate: A practical and powerful approach to multiple testing, J. Roy. Stat. Soc., 57B, 289–300, 1995.

Bintanja, R. and Selten, F. M.: Future increases in Arctic precipitation linked to local evaporation and sea-ice retreat, Nature, 509, 479–482, 2014.

Blackport, R. and Kushner, P. J.: The Transient and Equilibrium Climate Response to Rapid Summertime Sea Ice Loss in CCSM4, J. Climate, 29, 401–417, https://doi.org/10.1175/JCLI-D-15-0284.1, 2016.

Blackport, R. and Kushner, P. J.: Isolating the Atmospheric Circulation Response to Arctic Sea Ice Loss in the Coupled Climate System, Journal of Climate, 30, 2163–2185, https://doi.org/10.1175/JCLI-D-16-0257.1, 2017.

Blackport, R., Screen, J. A., van der Wiel, K., and Bintanja, R.: Minimal influence of reduced Arctic sea ice on coincident cold winters in mid-latitudes, Nature Climate Change, 9, 697–704, https://doi.org/10.1038/s41558-019-0551-4, 2019.

Blackport, R., Fyfe, J. C., and Screen, J. A.: Decreasing subseasonal temperature variability in the northern extratropics attributed to human influence, Nature Geoscience, 14, 719–723, https://doi.org/10.1038/s41561-021-00826-w, 2021.

Bouillon, S., Morales Maqueda, M. Á., Legat, V., and Fichefet, T.: An elastic-viscous-plastic sea ice model formulated on Arakawa B and C grids, Ocean Modelling, 27, 174–184, https://doi.org/10.1016/j.ocemod.2009.01.004, 2009.

Chernokulsky, A., Kozlov, F., Zolina, O., Bulygina, O., Mokhov, I. I., and Semenov, V. A.: Observed changes in convective and stratiform precipitation in Northern Eurasia over the last five decades, Environmental Research Letters, 14, 045 001, https://doi.org/10.1088/1748-9326/aafb82, 2019.

Cohen, J., Screen, J. A., Furtado, J. C., Barlow, M., Whittleston, D., Coumou, D., Francis, J., Dethloff, K., Entekhabi, D., Overland, J., and Jones, J.: Recent Arctic amplification and extreme mid-latitude weather, Nat. Geosci., 7, 627–637, http://dx.doi.org/10.1038/ngeo2234, 2014.

Cohen, J., Zhang, X., Francis, J., Jung, T., Kwok, R., Overland, J., Ballinger, T. J., Bhatt, U. S., Chen, H. W., Coumou, D., Feldstein, S., Gu, H., Handorf, D., Henderson, G., Ionita, M., Kretschmer, M., Laliberte, F., Lee, S., Linderholm, H. W., Maslowski, W., Peings, Y., Pfeiffer, K., Rigor, I., Semmler, T., Stroeve, J., Taylor, P. C., Vavrus, S., Vihma, T., Wang, S., Wendisch, M., Wu, Y., and Yoon, J.: Divergent consensuses on Arctic amplification influence on midlatitude severe winter weather, Nature Climate Change, 10, 20–29, https://doi.org/10.1038/s41558-019-0662-y, 2020.

Coumou, D. K., Di Capua, G., Vavrus, S., Wang, L., and Wang, S.: The influence of Arctic amplification on mid-latitude summer circulation, Nature Communications, 9, 2959, https://doi.org/10.1038/s41467-018-05256-8, 2018.

Craig, A., Valcke, S., and Coquart, L.: Development and performance of a new version of the OASIS coupler, OASIS3-MCT_3.0, Geoscientific Model Development, 10, 3297–3308, https://doi.org/10.5194/gmd-10-3297-2017, 2017.

Deser, C., Tomas, R., Alexander, M., and Lawrence, D.: The Seasonal Atmospheric Response to Projected Arctic Sea Ice Loss in the Late Twenty-First Century, J. Climate, 23, 333–351, http://dx.doi.org/10.1175/2009JCLI3053.1, 2010.

Deser, C., Tomas, R. A., and Sun, L.: The Role of Ocean–Atmosphere Coupling in the Zonal-Mean Atmospheric Response to Arctic Sea Ice Loss, J. Climate, 28, 2168–2186, http://dx.doi.org/10.1175/JCLI4278.1, 2015.

Ding, Q., Wallace, J. M., Battisti, D. S., Steig, E. J., Gallant, A. J. E., Kim, H.-J., and Geng, L.: Tropical forcing of the recent rapid Arctic warming in northeastern Canada and Greenland, Nature, 509, 209–212, https://doi.org/10.1038/nature13260, 2014.

Ding, Q., Schweiger, A., L'Heureux, M., Battisti, D., Po-Chedley, S., Johnson, N., Blanchard-Wrigglesworth, E., Harnos, K., Zhang, Q., Eastman, R., and Steig, E.: Influence of high-latitude atmospheric circulation changes on summertime Arctic sea ice, Nature Clim. Change, 7, 289–295, 2017.

Dobricic, S., Russo, S., Pozzoli, L., Wilson, J., and Vignati, E.: Increasing occurrence of heat waves in the terrestrial Arctic, Environmental Research Letters, 15, 024 022, https://doi.org/10.1088/1748-9326/ab6398, 2020.

Docquier, D., Grist, J. P., Roberts, M. J., Roberts, C. D., Semmler, T., Ponsoni, L., Massonnet, F., Sidoreno, D., Sein, D. V., Iovino, D., Bellucci, A., and Fichefet, T.: Impact of model resolution on Arctic sea ice and North Atlantic Ocean heat transport, Climate Dynamics, 53, 4989–5017, https://doi.org/10.1007/s00382-019-04840-y, 2019.

England, M., Polvani, L., and Sun, L.: Contrasting the Antarctic and Arctic Atmospheric Responses to Projected Sea Ice Loss in the Late Twenty-First Century, Journal of Climate, 31, 6353–6370, https://doi.org/10.1175/JCLI-D-17-0666.1, 2018.

Eyring, V., Bony, S., Meehl, G. A., Senior, C. A., Stevens, B., Stouffer, R. J., and Taylor, K. E.: Overview of the Coupled Model Intercomparison Project Phase 6 (CMIP6) experimental design and organization, Geoscientific Model Development, 9, 1937–1958, https://doi.org/10.5194/gmd-9-1937-2016, 2016.

Fichefet, T. and Morales Maqueda, M. : Sensitivity of a global sea ice model to the treatment of ice thermodynamics and dynamics, Journal of Geophysical Research, 1021, 12 609–12 646, https://doi.org/10.1029/97JC00480, 1997.

Folland, C. K., Knight, J., Linderholm, H. W., Fereday, D., Ineson, S., and Hurrell, J. W.: The Summer North Atlantic Oscillation: Past, Present, and Future, Journal of Climate, 22, 1082–1103, https://doi.org/10.1175/2008JCLI2459.1, 2009.

Ford, J. D., Smit, B., Wandel, J., Allurut, M., Shappa, K., Ittusarjuat, H., and Qrunnut, K.: Climate change in the Arctic: current and future vulnerability in two Inuit communities in Canada, The Geographical Journal, 174, 45–62, https://doi.org/https://doi.org/10.1111/j.1475-4959.2007.00249.x, 2008.

Francis, J. A. and Vavrus, S. J.: Evidence linking Arctic amplification to extreme weather in mid-latitudes, Geophys. Res. Lett., 39, L06 801, 2012.

Goosse, H., Arzel, O., Bitz, C. M., de Montety, A., and Vancoppenolle, M.: Increased variability of the Arctic summer ice extent in a warmer climate, Geophysical Research Letters, 36, https://doi.org/10.1029/2009GL040546, 2009.

Haarsma, R. J., Roberts, M. J., Vidale, P. L., Senior, C. A., Bellucci, A., Bao, Q., Chang, P., Corti, S., Fučkar, N. S., Guemas, V., von Hardenberg, J., Hazeleger, W., Kodama, C., Koenigk, T., Leung, L. R., Lu, J., Luo, J.-J., Mao, J., Mizielinski, M. S., Mizuta, R., Nobre, P., Satoh, M., Scoccimarro, E., Semmler, T., Small, J., and von Storch, J.-S.: High Resolution Model Intercomparison Project (HighResMIP v1.0) for CMIP6, Geoscientific Model Development, 9, 4185–4208, https://doi.org/10.5194/gmd-9-4185-2016, 2016.

Haug, T., Bogstad, B., Chierici, M., Gjøsæter, H., Hallfredsson, E. H., Åge S. Høines, Hoel, A. H., Ingvaldsen, R. B., Jørgensen, L. L., Knutsen, T., Loeng, H., Naustvoll, L.-J., Røttingen, I., and Sunnanå, K.: Future harvest of living resources in the Arctic Ocean north of the Nordic and Barents Seas: A review of possibilities and constraints, Fisheries Research, 188, 38–57, https://doi.org/https://doi.org/10.1016/j.fishres.2016.12.002, 2017.

Holland, M. M., Bitz, C. M., and Tremblay, B.: Future abrupt reductions in the summer Arctic sea ice, Geophysical Research Letters, 33, https://doi.org/10.1029/2006GL028024, 2006.

Hollowed, A. B., Planque, B., and Loeng, H.: Potential movement of fish and shellfish stocks from the sub-Arctic to the Arctic Ocean, Fisheries Oceanography, 22, 355–370, https://doi.org/https://doi.org/10.1111/fog.12027, 2013.

Horton, R. M., Mankin, J. S., Lesk, C., Coffel, E., and Raymond, C.: A Review of Recent Advances in Research on Extreme Heat Events, Current Climate Change Reports, 2, 242–259, https://doi.org/10.1007/s40641-016-0042-x, 2016.

Kharin, V., Zwiers, F., Zhang, X., and Wehner, M.: Changes in temperature and precipitation extremes in the CMIP5 ensemble, Climatic Change, 119, 345–357, https://doi.org/10.1007/s10584-013-0705-8, 2013.

Kharin, V. V., Flato, G. M., Zhang, X., Gillett, N. P., Zwiers, F., and Anderson, K. J.: Risks from Climate Extremes Change Differently from 1.5°C to 2.0°C Depending on Rarity, Earth's Future, 6, 704–715, https://doi.org/https://doi.org/10.1002/2018EF000813, 2018.

Kidston, J., Scaife, A. A., Hardiman, S. C., Mitchell, D. M., Butchart, N., Baldwin, M. P., and Gray, L. J.: Stratospheric influence on tropospheric jet streams, storm tracks and surface weather, Nature Geoscience, 8, 433–440, https://doi.org/10.1038/ngeo2424, 2015.

Kunkel, K. E., Pielke, R. A., and Changnon, S. A.: Temporal Fluctuations in Weather and Climate Extremes That Cause Economic and Human Health Impacts: A Review, Bulletin of the American Meteorological Society, 80, 1077 – 1098, https://doi.org/10.1175/1520-0477(1999)080<1077:TFIWAC>2.0.CO;2, 1999.

Landrum, L. and Holland, M.: Extremes become routine in an emerging new Arctic, Nature Climate Change, 10, 1108–1115, https://doi.org/10.1029/2020GL088583, 2020.

Madec, G.: NEMO Ocean ocean engine (Note du Pôle de modélisation, Institut Pierre-Simon Laplace (IPSL), France, No 27, ISSN No 1288-1619), 2016.

Madec, G., Benshila, R., Bricaud, C., Coward, A., Dobricic, S., Furner, R., and Oddo, P.: NEMO ocean engine, https://doi.org/10.5281/zenodo.1464817, revision 3797 from SVN repository (missing links), 2013.

Madec, G., Bourdallé-Badie, R., Bouttier, P.-A., Bricaud, C., Bruciaferri, D., Calvert, D., Chanut, J., Clementi, E., Coward, A., Delrosso, D., Ethé, C., Flavoni, S., Graham, T., Harle, J., Iovino, D., Lea, D., Lévy, C., Lovato, T., Martin, N., Masson, S., Mocavero, S., Paul, J., Rousset, C., Storkey, D., Storto, A., and Vancoppenolle, M.: NEMO ocean engine, https://doi.org/10.5281/zenodo.1472492, revision 8625 from SVN repository (missing links), 2017.

Manabe, S. and Stouffer, R. J.: Multiple-Century Response of a Coupled Ocean-Atmosphere Model to an Increase of Atmospheric Carbon Dioxide, Journal of Climate, 7, 5 – 23, https://doi.org/10.1175/1520-0442(1994)007<0005:MCROAC>2.0.CO;2, 1994.

Masson, V., Le Moigne, P., Martin, E., Faroux, S., Alias, A., Alkama, R., Belamari, S., Barbu, A., Boone, A., Bouyssel, F., Brousseau, P., Brun, E., Calvet, J.-C., Carrer, D., Decharme, B., Delire, C., Donier, S., Essaouini, K., Gibelin, A.-L., Giordani, H., Habets, F., Jidane, M., Kerdraon, G., Kourzeneva, E., Lafaysse, M., Lafont, S., Lebeaupin Brossier, C., Lemonsu, A., Mahfouf, J.-F., Marguinaud, P., Mokhtari, M., Morin, S., Pigeon, G., Salgado, R., Seity, Y., Taillefer, F., Tanguy, G., Tulet, P., Vincendon, B., Vionnet, V., and Voldoire, A.: The SURFEXv7.2 land and ocean surface platform for coupled or offline simulation of earth surface variables and fluxes, Geoscientific Model Development, 6, 929–960, https://doi.org/10.5194/gmd-6-929-2013, 2013.

Matthes, H., Rinke, A., and Dethloff, K.: Recent changes in Arctic temperature extremes: warm and cold spells during winter and summer, Environmental Research Letters, 10, 114 020, https://doi.org/10.1088/1748-9326/10/11/114020, 2015.

Meredith, M., Sommerkorn, M., Cassotta, S., Derksen, C., Ekaykin, A., Hollowed, A., Kofinas, G., Mackintosh, A., Melbourne-Thomas, J., Muelbert, M., Ottersen, G., Pritchard, H., and Schuur, E.: Polar Regions. In: IPCC Special Report on the Ocean and Cryosphere in a Changing Climate6 [Portner, H.-O., D.C. Roberts, V. Masson-Delmotte, P. Zhai, M. Tignor, E. Poloczanska, K. Mintenbeck, Alegria, M. Nicolai, A. Okem, J. Petzold, B. Rama, and N.M. Weyer (eds.)]., In Press, pp. 203–320, 2019.

Mogensen, K., Keeley, S., and Towers, P.: Coupling of the NEMO and IFS models in a single executable, p. 23, 2012.

Notz, D. and Stroeve, J.: Observed Arctic sea-ice loss directly follows anthropogenic CO2 emission, Science, 354, 747–750, https://doi.org/10.1126/science.aag2345, 2016.

Ogawa, F., Keenlyside, N., Gao, Y., Koenigk, T., Yang, S., Suo, L., Wang, T., Gastineau, G., Nakamura, T., Cheung, H. N., Omrani, N.-E., Ukita, J., and Semenov, V.: Evaluating Impacts of Recent Arctic Sea Ice Loss on the Northern Hemisphere Winter Climate Change, Geophysical Research Letters, 45, 3255–3263, https://doi.org/https://doi.org/10.1002/2017GL076502, 2018.

Onarheim, I. H., Eldevik, T., Smedsrud, L. H., and Stroeve, J. C.: Seasonal and Regional Manifestation of Arctic Sea Ice Loss, Journal of Climate, 31, 4917–4932, https://doi.org/10.1175/JCLI-D-17-0427.1, 2018.

Park, H.-S., Kim, S.-J., Seo, K.-H., Stewart, A. L., Kim, S.-Y., and Son, S.-W.: The impact of Arctic sea ice loss on mid-Holocene climate, Nature Communications, 9, 2018.

Peings, Y., Labe, Z. M., and Magnusdottir, G.: Are 100 Ensemble Members Enough to Capture the Remote Atmospheric Response to +2°C Arctic Sea Ice Loss?, Journal of Climate, 34, 3751 – 3769, https://doi.org/10.1175/JCLI-D-20-0613.1, 2021.

Petoukhov, V. and Semenov, V. A.: A link between reduced Barents-Kara sea ice and cold winter extremes over northern continents, Journal of Geophysical Research: Atmospheres, 115, https://doi.org/10.1029/2009JD013568, 2010.

Pithan, Y. and Mauritsen, T.: Arctic amplification dominated by temperature feedbacks in contemporary climate models, Nature Geoscience, 7, 181–184, https://doi.org/10.1175/JCLI-D-13-00272.1, 2014.

Richter, J. H., Anstey, J. A., Butchart, N., Kawatani, Y., Meehl, G. A., Osprey, S., and Simpson, I. R.: Progress in Simulating the Quasi-Biennial Oscillation in CMIP Models, Journal of Geophysical Research: Atmospheres, 125, e2019JD032 362, https://doi.org/https://doi.org/10.1029/2019JD032362, e2019JD032362 10.1029/2019JD032362, 2020.

Ritchie, H., Temperton, C., Simmons, A., Hortal, M., Davies, T., Dent, D., and Hamrud, M.: Implementation of the semi-Lagrangian method in a high-resolution version of the ECMWFforecast model, Weather Rev, 123, 489–514, 1995.

Roberts, C. D., Senan, R., Molteni, F., Boussetta, S., Mayer, M., and Keeley, S. P. E.: Climate model configurations of the ECMWF Integrated Forecasting System (ECMWF-IFS cycle 43r1) for HighResMIP, Geoscientific Model Development, 11, 3681–3712, https://doi.org/10.5194/gmd-11-3681-2018, 2018.

Screen, J., Deser, C., Simmonds, I., and Tomas, R.: Atmospheric impacts of Arctic sea-ice loss, 1979–2009: separating forced change from atmospheric internal variability, 43, 333–344–, http://dx.doi.org/10.1007/s00382-013-1830-9, 2014.

Screen, J. A. and Simmonds, I.: The central role of diminishing sea ice in recent Arctic temperature amplification, Nature, 464, 1334–1337, 2010.

Screen, J. A., Deser, C., and Sun, L.: Projected changes in regional climate extremes arising from Arctic sea ice loss, Environmental Research Letters, 10, 084 006, https://doi.org/10.1088/1748-9326/10/8/084006, 2015.

Screen, J. A., Deser, C., Smith, D. M., Zhang, X., Blackport, R., Kushner, P. J., Oudar, T., McCusker, K. E., 6, and Sun, L.: Consistency and discrepancy in the atmospheric response to Arctic sea-ice loss across climate models, Nat. Geosci., 11, 155–163, doi: 10.1038/s41561-018-0059-y, 2018.

Semmler, T., McGrath, R., and Wang, S.: The impact of Arctic sea ice on the Arctic energy budget and on the climate of the Northern mid-latitudes, Climate Dynamics, 39, 2675–2694, https://doi.org/10.1007/s00382-012-1353-9, 2012.

Semmler, T., Stulic, L., Jung, T., Tilinina, N., Campos, C., Gulev, S., and Koracin, D.: Seasonal Atmospheric Responses to Reduced Arctic Sea Ice in an Ensemble of Coupled Model Simulations, J. Climate, 29, 5893–5913, https://doi.org/10.1175/JCLI-D-15-0586.1, 2016.

Sillmann, J., Kharin, V. V., Zhang, X., Zwiers, F. W., and Bronaugh, D.: Climate extremes indices in the CMIP5 multimodel ensemble: Part 1. Model evaluation in the present climate, J Geophys Res, 118, 1716–1733, https://doi.org/10.1002/jgrd.50203, 2013a.

Sillmann, J., Kharin, V. V., Zwiers, F. W., Zhang, X., and Bronaugh, D.: Climate extremes indices in the CMIP5 multimodel ensemble: Part 2. Future climate projections, Journal of Geophysical Research: Atmospheres, 118, 2473–2493, https://doi.org/https://doi.org/10.1002/jgrd.50188, 2013b.

SIMIP, C.: Arctic Sea Ice in CMIP6, Geophysical Research Letters, 47, e2019GL086 749, https://doi.org/10.1029/2019GL086749, 2020.

Smith, D. M., Dunstone, N. J., Scaife, A. A., Fiedler, E. K., Copsey, D., and Hardiman, S. C.: Atmospheric Response to Arctic and Antarctic Sea Ice: The Importance of Ocean–Atmosphere Coupling and the Background State, J. Climate, 30, 4547–4565, https://doi.org/10.1175/JCLI-D-16-0564.1, 2017.

Smith, D. M., Screen, J. A., Deser, C., Cohen, J., Fyfe, J. C., García-Serrano, J., Jung, T., Kattsov, V., Matei, D., Msadek, R., Peings, Y., Sigmond, M., Ukita, J., Yoon, J.-H., and Zhang, X.: The Polar Amplification Model Intercomparison Project (PAMIP) contribution to CMIP6: investigating the causes and consequences of polar amplification, Geoscientific Model Development, 12, 1139–1164, https://doi.org/10.5194/gmd-12-1139-2019, 2019.

Stevenson, K. T., RADER, H. B., ALESSA, L., KLISKEY, A. D., PANTOJA, A., CLARK, M., SMEENK, J., and Giguère, N.: Sustainable Agriculture for Alaska and the Circumpolar North: Part II. Environmental, Geophysical, Biological and Socioeconomic Challenges, Arctic, 67, 296–319, 2014.

Streffing, J., Semmler, T., Zampieri, L., and Jung, T.: Response of Northern Hemisphere Weather and Climate to Arctic Sea Ice Decline: Resolution Independence in Polar Amplification Model Intercomparison Project (PAMIP) Simulations, Journal of Climate, 34, 8445 – 8457, https://doi.org/10.1175/JCLI-D-19-1005.1, 2021.

Sun, L., Deser, C., Tomas, R. A., and Alexander, M.: Global Coupled Climate Response to Polar Sea Ice Loss: Evaluating the Effectiveness of Different Ice-Constraining Approaches, Geophysical Research Letters, 47, e2019GL085 788, https://doi.org/https://doi.org/10.1029/2019GL085788, e2019GL085788 2019GL085788, 2020.

Swart, N. C., Fyfe, J. C., Hawkins, E., Kay, J. E., and Jahn, A.: Influence of internal variability on Arctic sea-ice trends, Nature Climate Change, 5, 86–89, https://doi.org/10.1038/nclimate2483, 2015.

Temperton, C., Hortal, M., and Simmons, A.: A two-time-level semi-Lagrangian global spectral model, pp. 111–127, 2001.

Voldoire, A., Saint-Martin, D., Sénési, S., Decharme, B., Alias, A., Chevallier, M., Colin, J., Guérémy, J.-F., Michou, M., Moine, M.-P., Nabat, P., Roehrig, R., Salas y Mélia, D., Séférian, R., Valcke, S., Beau, I., Belamari, S., Berthet, S., Cassou, C., Cattiaux, J., Deshayes, J., Douville, H., Ethé, C., Franchistéguy, L., Geoffroy, O., Lévy, C., Madec, G., Meurdesoif, Y., Msadek, R., Ribes, A., Sanchez-Gomez, E., Terray, L., and Waldman, R.: Evaluation of CMIP6 DECK Experiments With CNRM-CM6-1, Journal of Advances in Modeling Earth Systems, 11, 2177–2213, https://doi.org/10.1029/2019MS001683, 2019.

Walsh, J. E., Fetterer, F., Scott Stewart, J., and Chapman, W. L.: A database for depicting Arctic sea ice variations back to 1850, Geographical Review, 107, 89–107, https://doi.org/https://doi.org/10.1111/j.1931-0846.2016.12195.x, 2017.

Wilks, D. S.: "The Stippling Shows Statistically Significant Grid Points": How Research Results are Routinely Overstated and Overinterpreted, and What to Do about It, Bulletin of the American Meteorological Society, 97, 2263–2273, https://doi.org/10.1175/BAMS-D-15-00267.1, 2016.

Zhang, J. and Rothrock, D. A.: Modeling Global Sea Ice with a Thickness and Enthalpy Distribution Model in Generalized Curvilinear Coordinates, Monthly Weather Review, 131, 845 – 861, https://doi.org/10.1175/1520-0493(2003)131<0845:MGSIWA>2.0.CO;2, 2003.

Zhang, X., Alexander, L., Hegerl, G. C., Jones, P., Tank, A. K., Peterson, T. C., Trewin, B., and Zwiers, F. W.: Indices for monitoring changes in extremes based on daily temperature and precipitation data, WIREs Climate Change, 2, 851–870, https://doi.org/https://doi.org/10.1002/wcc.147, 2011.